

Chapter 4

Quantum correction to the Pair Distribution Function calculated classically.

4.1 Introduction

Recently, due to the subtleness of the protein folding problem especially, there is a demand for different techniques that will allow an accurate study of molecular structures and their dynamics, yet will not require time-consuming calculations, at least for relatively small molecules.

The pair distribution function (PDF), that can be obtained by Fourier transform of powder diffraction data, traditionally has been to describe short-range correlations in atomic positions.

In recent years a technique has been developed that allows one to achieve an extremely good agreement between calculated and experimental PDFs for crystalline materials. [59, 36, 37].

Molecular Dynamics or Monte Carlo techniques are usually implemented in order

to study molecular structures and their dynamics. Thus, quantum effects are usually ignored. Other approaches, like the Car-Parinello method [60], that are based on quantum mechanics, are more time consuming than classical approaches and only feasible for a small number of atoms.

Accurate experimental PDFs can be obtained from X-ray or neutron diffraction experiments. Thus, in order to use PDFs to compare modeled molecular structures and their dynamics with real molecular structures and their motion, it is necessary to calculate molecular PDFs accurately. It is possible that PDFs obtained in classical calculations, in ignorance of QM effects, do not provide sufficient accuracy any more.

Thus, it is important to estimate the role of QM effects in calculations of PDF for molecules. Further, we will see that the accuracy of PDFs calculated using classical methods can be significantly improved without switching to QM calculations completely, but by implementing some quantum corrections to classically calculated PDFs.

It is known, that even at zero temperature, if it would be accessible, atoms would vibrate near their equilibrium positions due to the completely quantum effect that is called zero-point motion [63, 64]. This effect is completely missing in classical MC or MD calculations.

As was already discussed in the previous chapters, the width of the peaks in the PDF of solid materials is determined by the mean square deviation of the distance between a pair of atoms from its equilibrium value. Thus, at low temperatures especially, ignorance of zero point motion in classical calculations should result in a peak-width that is (significantly) smaller than the one that occurs in reality.

In this chapter the role of atomic zero point motion is discussed. The size of the effect is estimated by comparing the dependencies of the mean square displacements of a particle in the Morse potential on temperature in QM and CM calculations. We used a Morse potential because it was developed and proved to be useful in modelling

the properties of diatomic molecules. This potential is also convenient because it allows an exact QM solution. After that we develop a technique that allows to take into account the effect of zero point motion in PDFs calculated classically for more complex molecules. The same method is used to correct the classically calculated heat capacitance.

Usually, even in very simple molecules, there are different energy scales associated with the bond-stretching, angle-bending, dihedral angles rotations and so on. Although our correction can be applied to all pairs of atoms, it is the most important for those pairs that strongly interact with each other so that the energy associated with this pair (at a given temperature) is still almost the ground state energy of the corresponding vibrational mode. Thus, our correction is most important for those pairs of atoms that are close to each other, while the atoms that are further away could be treated classically. It means that the correction affects mostly the shape of PDF at smaller distances.

Molecules are usually in some environment that also contributes to the value of PDF at a particular distance. Often there are many molecules that form a liquid. Intermolecular interactions are usually much weaker than intramolecular interactions and thus they can be treated mostly classically, i.e. with MC or MD technique. In order to calculate accurately the PDF for a real samples it is necessary first of all to be able to calculate accurately the PDF for a single isolated molecule. That is the question that we address in this chapter.

Thus, our technique suggests the following algorithm for more accurate calculations of PDFs. The initial PDF can be extracted from classical MC or MD simulations that provide coordinates of atoms in a molecule as a functions of time, i.e. molecular trajectory. This modeled PDF already can be compared with the experimental PDF. Then, in order to achieve a better agreement between modeled and experimental PDFs quantum correction can be applied to the PDF obtained from classical

simulations.

In this chapter, we at first consider the case of exactly solvable Morse potential for a diatomic molecule. We use this example to demonstrate the precision of classical calculations of PDF and the importance of the quantum correction. Another quantity that can be corrected with our method is the heat capacitance that was calculated by classical methods.

After that, in an attempt to use our correction for more complex molecules, we apply our method to the C_6H_{14} molecule. At first we study the role of quantum corrections at very low temperatures when the molecule is in one of the equilibrium configurations and it can be assumed that the atoms only slightly vibrate near about their equilibrium positions. If the amplitudes of atomic vibrations are small enough, it can be assumed that their motion is harmonic. In this case the problem could be solved exactly using either classical or quantum approaches. Thus, the role of quantum effects can be estimated at different temperatures. Finally, we calculate the PDF for the C_6H_{14} molecule at higher temperatures when the potential cannot be considered as harmonic any more and at even higher temperatures, when the molecule becomes flexible.

In our calculations we used the “TINKER” molecular dynamics simulation package that can search for equilibrium configurations and calculate eigenfrequencies and eigenvectors of molecular vibrations in these configurations. It was also used to run molecular dynamics simulations at a particular temperature. The obtained molecular trajectories (coordinates of atoms as a function of time) were used in calculations of PDF.

4.2 Pair Distribution Function for a single molecule

The experimental PDF function $G_{ex}(r)$ is obtained from the powder diffraction data via a sine Fourier transform of the normalized scattering intensity $S(Q)$:

$$G_{ex}(r) = \frac{2}{\pi} \int_0^{\infty} Q[S(Q) - 1] \sin(Qr) dQ \quad (4.1)$$

where Q is the magnitude of the scattering vector. For elastic scattering $Q = 4\pi \sin \theta / \lambda$ with 2θ being the scattering angle and λ the wavelength of the radiation used.

On the other hand, the PDF is related to the structure of the material. The PDF is simply the bond length distribution of the material weighted by the respective scattering powers of the contributing atoms. It can be calculated from the structural model using the relation:

$$G_c(r) = 4\pi r \left\{ \left[\frac{1}{4\pi r^2} \sum_i \sum_j \frac{b_i b_j}{\langle b^2 \rangle} \delta(r - r_{ij}) \right] - \rho_o \right\}, \quad (4.2)$$

where the sum goes over all pairs of atoms i and j separated by r_{ij} within the model sample. The scattering power of the atom i is b_i and $\langle b^2 \rangle$ is the average scattering power of the sample. In the case of neutron scattering b_i is simply the scattering length, whereas in the case of X-rays it is the atomic form factor evaluated at a given value of Q . For $Q = 0$ the value b_i is simply the number of electrons of atom i .

The first term in square brackets in (4.2) represents radial density $\rho(r)$ normalized in such a way that the number of atoms in the spherical annulus of thickness dr is given by $4\pi r^2 \rho(r) dr$. In solid materials, where atoms vibrate near their equilibrium positions $\delta(r - r_{ij})$ -functions in (4.2) should be substituted with Gaussians, whose width σ_{ij}^2 is determined by the mean square deviation of the r_{ij} from its equilibrium value: $\sigma_{ij}^2 = \langle (r_{ij} - \bar{r}_{ij})^2 \rangle$. For our purposes it is convenient to define, instead of

$G_c(r)$, a different function $g(r)$ to which we will refer to as the PDF. Summarizing we can write:

$$g(r) \equiv 4\pi r^2 \rho(r) = \sum_i \sum_j \frac{b_i b_j}{\langle b \rangle^2} \frac{\exp\left[-\frac{(r-\bar{r}_{ij})^2}{2\sigma_{ij}^2}\right]}{\sqrt{2\pi\sigma_{ij}^2}} \quad (4.3)$$

In order to accurately calculate PDF it is necessary, in particular, accurately calculate the peak width σ_{ij}^2 for the atoms that belong to the same molecule. That is the issue that we discuss in this work.

Substitution of δ -functions with Gaussians occurs due to the time averaging of the distances between atomic pairs. If vibrations would not be small, for example if a molecule becomes flexible, δ -functions should be substituted not by Gaussians, but by normalized probabilities to atoms in the pair at a given distance. For a particular pair, the shape of the probability function can be rather complicated. For example, it can contain several peaks that correspond to the different equilibrium configurations.

4.3 An example of Morse potential. The idea of the method.

Assume, for simplicity, that we are interested in an accurate calculation of the PDF for a diatomic molecule. Also assume that the only variable on which potential energy U depends is the deviation $x = r - r_o$ of the distance r between the atoms from its equilibrium value r_o . If there is only one minimum in $U = U(x)$ then the molecule has only one vibrational mode.

In the center of the mass the Hamiltonian of the system can be written as:

$$H = \frac{p^2}{2\mu} + U(x), \quad (4.4)$$

where $\mu = m/2$ is the reduced mass.

In the limits of low and high temperatures, this problem could be solved approximately. At low temperatures, when the deviation of the distance between the pair of atoms from its equilibrium value is very small, instead of the potential $U(x)$ we use the harmonic approximation:

$$U_H(x) \simeq U_o + \frac{\mu\omega^2(x - x_o)^2}{2}, \quad (4.5)$$

so that we can write:

$$H = \frac{p^2}{2\mu} + \frac{\mu\omega^2(x - x_o)^2}{2}. \quad (4.6)$$

(It can be assumed, without changes in the results that $U_o = 0$) The solution of the problem in the harmonic approximation is well known. The energy levels are given by:

$$E_n = \hbar\omega[n + \frac{1}{2}]. \quad (4.7)$$

In the harmonic potential the average values of kinetic and potential energies are the same: $\langle E_{kin} \rangle = \langle E_{pot} \rangle = E_{tot}/2$. Thus

$$\langle \frac{p^2}{2\mu} \rangle = \langle \frac{\mu\omega^2(x - x_o)^2}{2} \rangle = \frac{1}{2}\hbar\omega[n + \frac{1}{2}]. \quad (4.8)$$

From this we get:

$$\sigma_{HQM}^2(T) \equiv \langle (x - x_o)^2 \rangle = \frac{\hbar}{\mu\omega}[n + \frac{1}{2}], \quad (4.9)$$

where abbreviation HQM stands for Harmonic Quantum Mechanics. The Bose-

Einstein function $n(T)$ is given by:

$$n(T) = \frac{1}{\exp\left[\frac{\hbar\omega}{k_bT}\right] - 1}. \quad (4.10)$$

Expanding this at high temperatures $(\hbar\omega)/(k_bT) \ll 1$ we get:

$$n(T) \cong \frac{k_bT}{\hbar\omega} - \frac{1}{2}, \quad (4.11)$$

Thus, at high temperatures:

$$\langle (x - x_o)^2 \rangle = \frac{\hbar}{\mu\omega} \frac{k_bT}{\hbar\omega} = \frac{k_bT}{\mu\omega^2} \quad (4.12)$$

If the spacing between the energy levels $\Delta E = \hbar\omega$ is much smaller than k_bT (i.e. $\hbar\omega/k_bT \ll 1$) the problem could be solved classically. In the last case, the probability to find the particle at some coordinate x is given by the Boltzman probability:

$$P_{CM}(x, T) = \frac{1}{Z_{CM}} \exp\left[-\frac{U(x)}{k_bT}\right], \quad (4.13)$$

where

$$Z_{CM} = \int \exp\left[-\frac{U(x)}{k_bT}\right] dx. \quad (4.14)$$

So that:

$$\langle x \rangle = \int x P_{CM}(x, T), \quad (4.15)$$

and

$$\langle x^2 \rangle = \int x^2 P_{CM}(x, T). \quad (4.16)$$

Thus:

$$\sigma_{CM}^2(T) = \langle (x - \langle x \rangle)^2 \rangle = \langle x^2 \rangle - \langle x \rangle^2 \quad (4.17)$$

could be found. In the harmonic case, ($U(x) = \mu\omega^2(x - x_o)^2/2$): $\langle x \rangle = x_o$, $Z = \sqrt{2\pi k_b T / \mu\omega^2}$ and $\sigma_{HCM}^2(T) = k_b T / \mu\omega^2$, which is the same result as (4.12).

At higher temperatures, when the amplitudes of atomic vibrations are larger, it may not be appropriate to use the harmonic approximation for $U(x)$. Instead, it is necessary to solve the problem for the original potential $U(x)$. Again, as before, if the spacing between the energy levels is much bigger than $k_b T$ the problem should be solved quantum mechanically. In the opposite limit $\Delta E \ll k_b T$ the classical solution could be employed.

There is another potential $U(x)$ that allows the exact QM solution. That is the Morse potential[65], which is widely used to model the properties of diatomic molecules:

$$\begin{aligned} U_M(x) &= -U_{min} + U_o \{1 - \exp[-\alpha x]\}^2 \\ &= (-U_{min} + U_o) + U_o [\exp[-2\alpha x] - 2\exp[-\alpha x]] \end{aligned} \quad (4.18)$$

In this potential there is a finite number of the energy levels in the discrete specter.

The values of the energies are given by:

$$E_n = (-U_{min} + U_o) - U_o \left[1 - \frac{\alpha \hbar}{\sqrt{2mU_o}} \left(n + \frac{1}{2}\right)\right]^2, \quad (4.19)$$

where n runs over the positive integer values from zero to the maximum value at which the term in the square brackets is still positive.

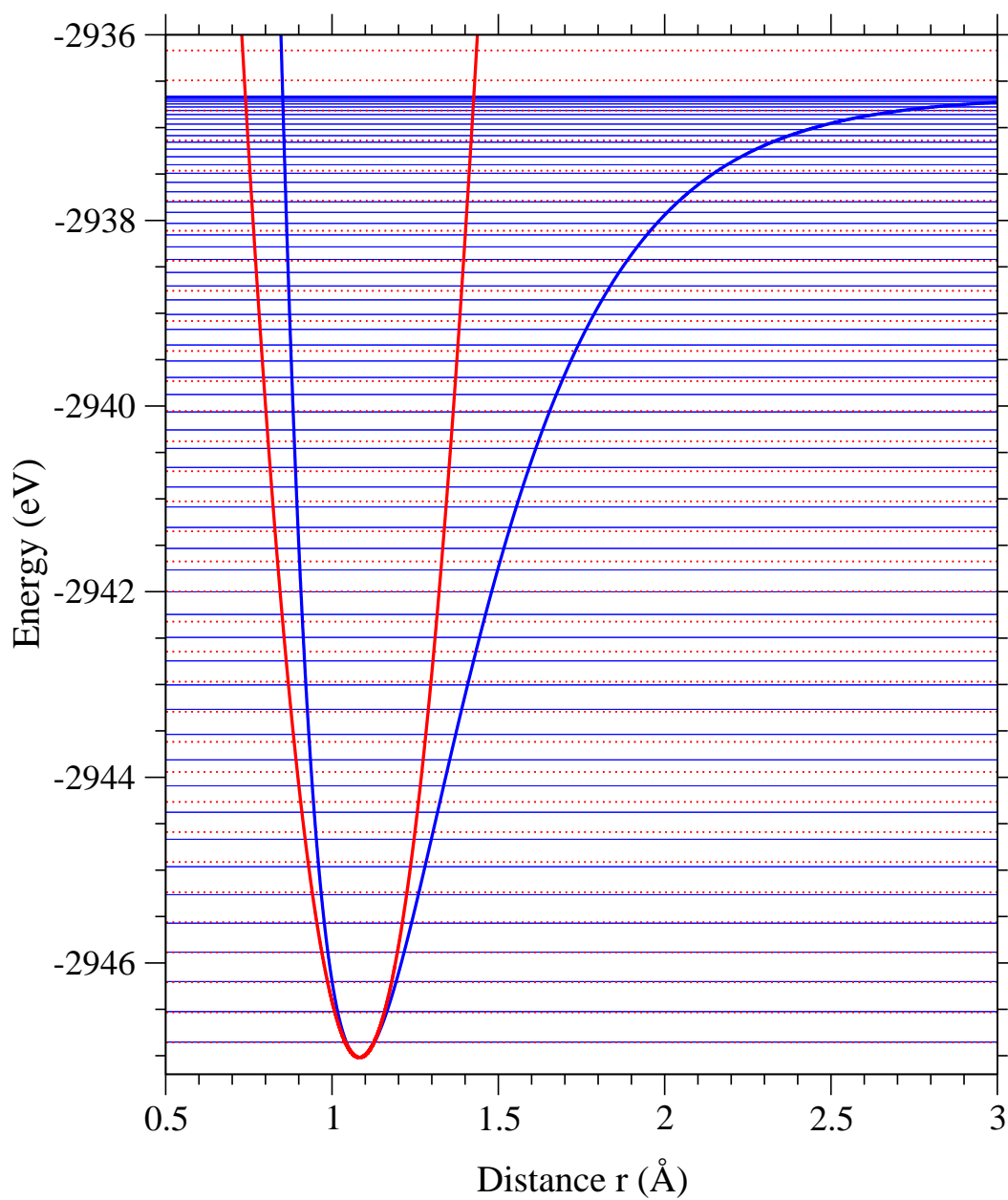


Figure 4.1: The blue curve shows the Morse potential for the N_2 molecule. The red curve shows the harmonic approximation to the Morse potential at small values of x . The blue and red horizontal lines are the energy levels for the Morse and harmonic potentials respectively.

The non-normalized wave functions are given by:

$$\psi_n(x) = \exp\left[-\frac{\xi^2}{2}\right] \xi^s w_n(\xi), \quad (4.20)$$

where

$$\xi = \frac{2\sqrt{2mU_o}}{\alpha\hbar} \exp(-\alpha x), \quad (4.21)$$

and

$$s = \frac{\sqrt{2mU_o}}{\alpha\hbar} - \left(n + \frac{1}{2}\right). \quad (4.22)$$

Finally $w_n(\xi) = F(-n, 2s + 1, \xi)$ is the confluent hypergeometric function that can be found by the series:

$$\begin{aligned} F(\alpha, \gamma, z) &= 1 + \frac{\alpha}{\gamma} \frac{z}{1!} + \frac{\alpha(\alpha+1)}{\gamma(\gamma+1)} \frac{z^2}{2!} \\ &+ \frac{\alpha(\alpha+1)(\alpha+2)}{\gamma(\gamma+1)(\gamma+2)} \frac{z^3}{3!} + \frac{\alpha(\alpha+1)(\alpha+2)(\alpha+3)}{\gamma(\gamma+1)(\gamma+2)(\gamma+3)} \frac{z^4}{4!} + \dots \end{aligned} \quad (4.23)$$

In our case, when $\alpha = -n$, the confluent hypergeometric function is a polynomial of degree n .

If the energy levels and the wave functions are known, the probability to find the particle at temperature T at position x is given by:

$$P_{QM}(x, T) = \frac{1}{Z_{QM}} \sum_{n=0}^{n_{max}} |\psi_n(x)|^2 \exp\left[-\frac{E_n}{k_b T}\right], \quad (4.24)$$

where

$$Z_{QM} = \sum_{n=0}^{n_{max}} \exp\left[-\frac{E_n}{k_b T}\right]. \quad (4.25)$$

Then $\langle x \rangle$ and $\langle x^2 \rangle$ could be found as:

$$\langle x_{QM}(T) \rangle = \int x P_{QM}(x) dx, \quad (4.26)$$

and

$$\langle x_{QM}^2(T) \rangle = \int x^2 P_{QM}(x) dx. \quad (4.27)$$

Finally from (4.26,4.27) we get:

$$\sigma_{QM}^2(T) = \langle (x - \bar{x})^2 \rangle = \langle x_{QM}^2(T) \rangle - \langle x_{QM}(T) \rangle^2. \quad (4.28)$$

In these calculations the continuous spectrum was ignored. Thus, being exact at low temperatures these QM calculations should fail at very high temperatures.

For the harmonic potential, the sums (4.24, 4.25) could be explicitly calculated [64] with the following result:

$$P_{HQM}(x, T) = \left(\frac{\alpha}{\pi}\right)^{\frac{1}{2}} \exp[-\alpha x^2], \quad (4.29)$$

where

$$\alpha = \frac{m\omega}{\hbar} \tanh\left[\frac{\hbar\omega}{2k_b T}\right]. \quad (4.30)$$

If the temperature is high enough, instead the Boltzman probability (4.13, 4.14, 4.17) with $U(x) = U_M(x)$ could be used to calculate σ^2 . MC and MD simulations, being classical, produce σ^2 that correspond to the Boltzman distribution at all temperatures. Thus, their results are not valid at very low temperatures.

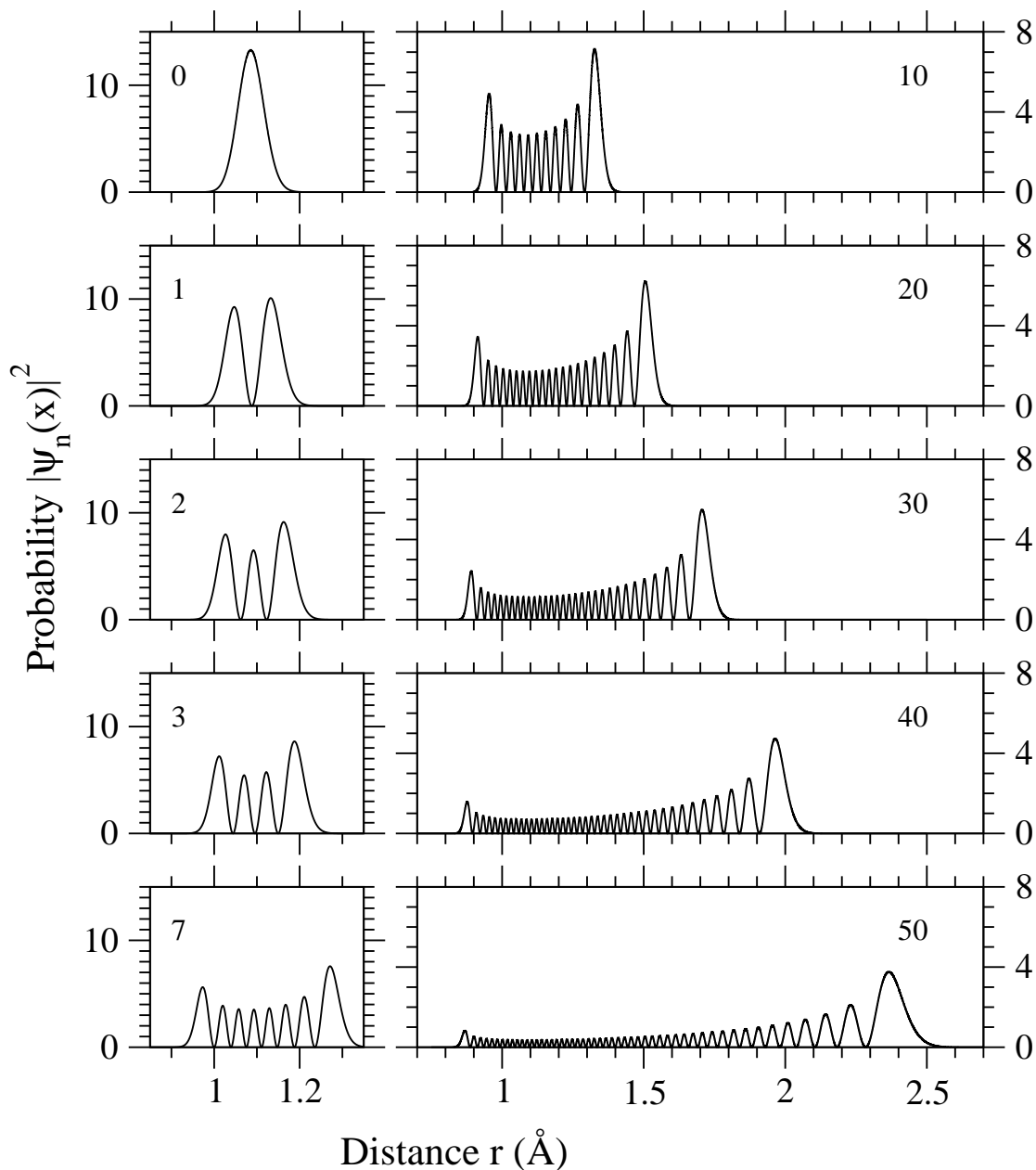


Figure 4.2: The squares of the wave functions of the Morse potential for the N_2 molecule. The little figures on the left from the top to the bottom show normalized wave functions for $n = 0, 1, 2, 3, 7$. The figures on the right from the top to the bottom show normalized wave functions for $n = 10, 20, 30, 40, 50$. There are 61 energy levels for the chosen values of parameters.

4.3.1 Molecule N_2

As an example, we consider the Morse potential $U_M(x)$ parameterized for the N_2 molecule. The blue curve on Fig.4.1 shows the corresponding Morse potential. It was obtained by performing calculations with the Gaussian98 [61, 62] program that was approximately solving the Schrödinger equation for the electrons when the distance between the nucleus of N atoms was fixed. The equilibrium distance $r_o = 1.0828 \text{ \AA}$ and the equilibrium energy $U_{min} = 2947.0188 \text{ eV}$ were found in a separate optimization run. In the same way, the energies E_N of the individual N atoms were calculated. Double of this energy is $2E_N = -U_{min} + U_o = -2936.6608 \text{ eV}$. This information is sufficient to construct Morse potential (4.18). The red curve is the harmonic approximation for the Morse potential at small values of $x = r - r_{min}$. The blue horizontal lines are the quantum energy levels of the Morse potential, while the red dashed lines are the energy levels of the corresponding harmonic potential. For the used values of parameters, there are 61 energy levels in the Morse potential.

The squares of the normalized wave functions of the Morse potential for the N_2 molecule are shown in Fig. 4.2. The wave functions corresponding to $n = 0, 1, 2, 3, 7$ are on the left and for $n = 10, 20, 30, 40, 50$ are on the right. Thus, for small n the particle could be found only near the minimum of the potential r_o . As n increases, due to the asymmetry of the potential, the probability density, as well as $\langle r \rangle$ shifts to the right, and thus the particle spends more and more time away from the minimum.

Figure 4.3 shows probabilities to find the particle at a given distance in the Morse potential and its harmonic approximation at different temperatures. For a diatomic molecule these probabilities represent the pair distribution function. At very low temperatures the CM results for Morse potential and its harmonic approximation almost coincide. However, the QM results are different. In QM, the ground state energies for the Morse and Harmonic potentials are separated from the bottom of the

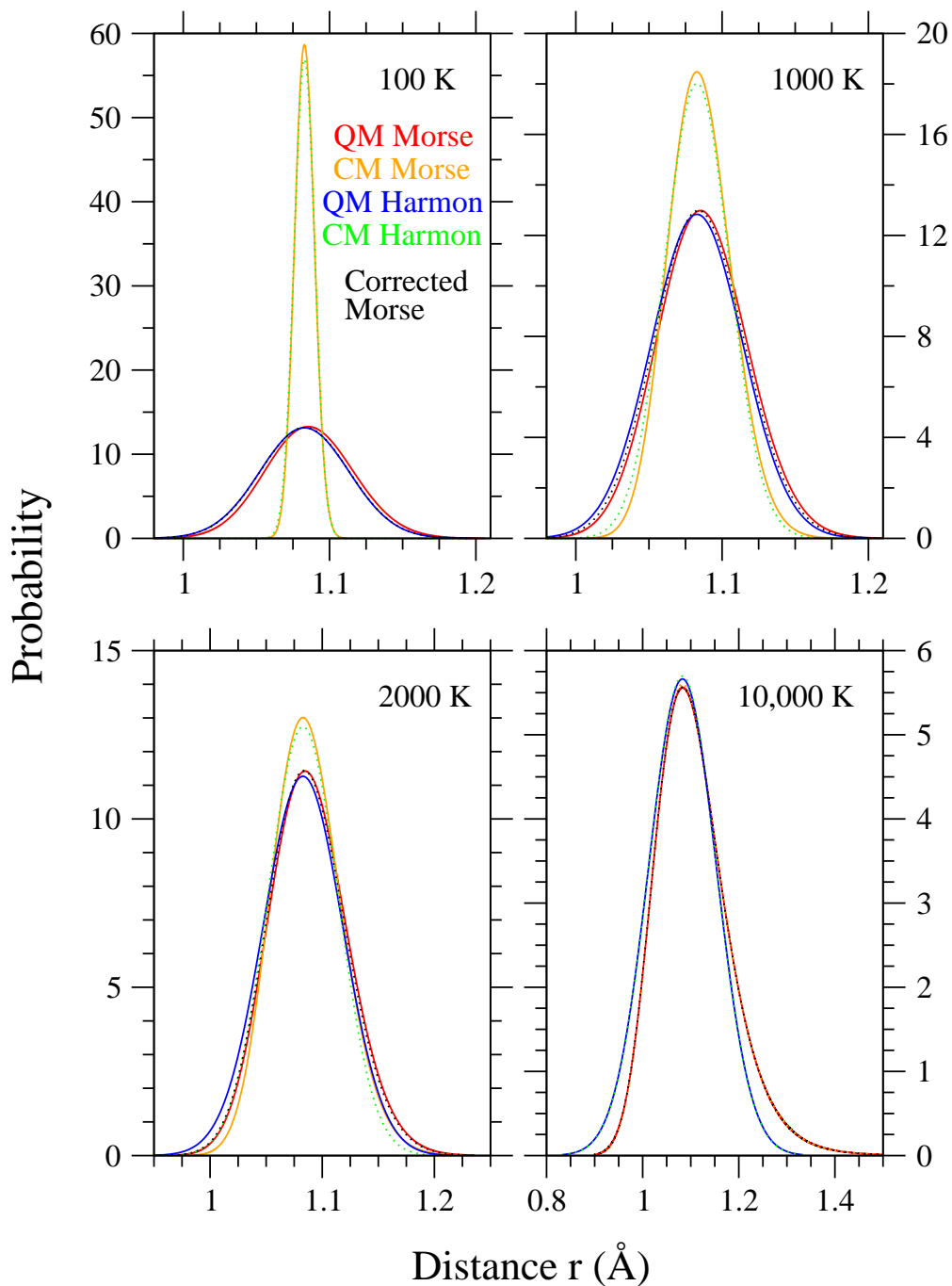


Figure 4.3: The Pair Distribution Functions or the probabilities to find the particle at a given distance in the Morse potential or its harmonic approximation at temperatures 100K, 1000K, 2000K and 10,000K. The red and orange curves represent QM (4.24,4.25) and CM (4.13,4.14) results for the Morse potential. The blue and green curves represent QM and CM results for the harmonic approximation to the Morse potential. The black curves represent CM results for the Morse potential corrected by the convolution (4.34) with σ_{corr}^2 obtained from the harmonic approximation to the Morse potential.

potential by finite (slightly different) energy values. Because of it the anharmonicity of the Morse potential is reflected even in the ground state of the particle. This leads to the slightly different PDFs that were obtained using QM on the Morse and harmonic potentials. At temperature 10,000K the non-Gaussian line shape of the PDFs obtained on the Morse potential are well pronounced. The depth of the Morse potential corresponds to $\approx 100,000$ K

Figure 4.4 shows dependencies of $\sigma^2(T)$ on temperature T that were calculated in four different ways. The red curve shows the result of the QM calculation for the Morse potential, where the summation in (4.24,4.25) were performed (numerically) over the 61 energy levels. At the temperatures plotted $T < 10,000$ K this result is not any different from the result that could be obtained by the summation over the first 35 energy levels. Thus, it can be assumed that the range of integration in (4.28) is $(-\infty, \infty)$, while for the calculation the range $(0.5, 2.5)$ Å was used. The orange curve shows the result of CM calculations of $\sigma^2(T)$ for the Morse potential (4.13,4.14,4.17). There is a subtle point concerning the range of the integration in (4.17). This question is discussed in Appendix B. The blue and green curves show QM (4.9) and CM (4.12) results for the harmonic potential.

Note that $\sigma_{CM}^2(T)$ calculated classically for both: the Morse and Harmonic potentials, converges to zero as $T \rightarrow 0$. In contrast, $\sigma_{QM}^2(T)$ calculated by QM methods for both potentials converge to a finite non-zero value as $T \rightarrow 0$. This is the effect called zero-point motion. In other words, atoms in QM are not motionless even at zero temperature.

Classical MD or MC simulations performed on the Morse and Harmonic potentials would lead to the orange and green curves respectively. Thus, classical methods lead, especially at low temperature, to significantly incorrect results. In order to obtain the correct results, it is necessary to use the QM approach.

Potentials that are used to model molecular motion for complicated molecules

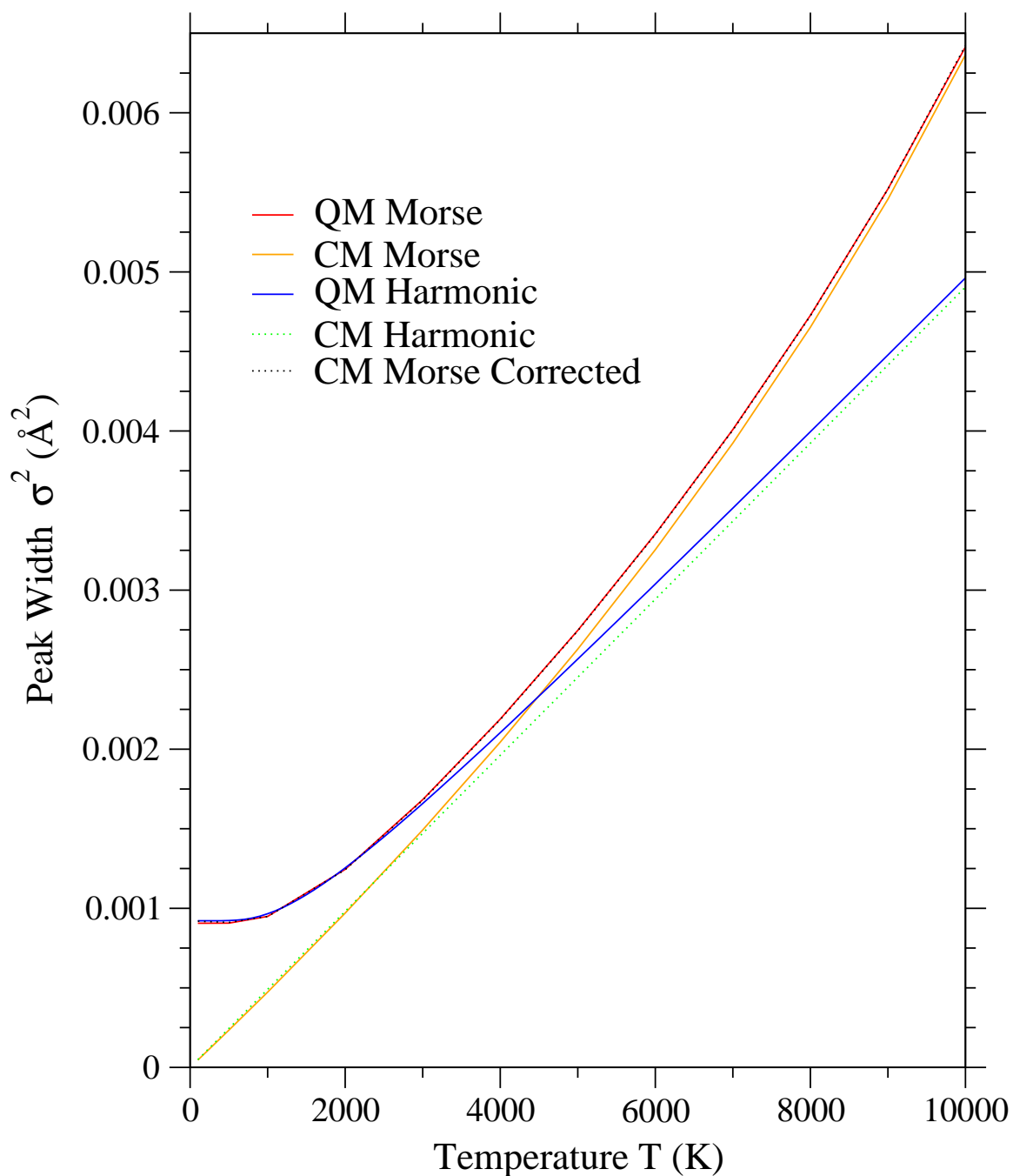


Figure 4.4: The dependencies of σ^2 on temperature T that were calculated in four different ways. The red and orange curves show QM (4.24, 4.25, 4.28) and CM (4.13, 4.14, 4.17) results for the Morse potential. The blue and green curves show QM (4.9) and CM (4.12) results for the harmonic approximation to the Morse potential. The black curve shows the CM results on the Morse potential with correction (4.31) that comes from the harmonic approximation to the Morse potential.

do not allow exact QM calculations. The harmonic approximation still could be used to solve the problem at low temperatures. It can be employed if equilibrium configurations, vibrational frequencies and vibrational eigenvectors are known. In this case, it is possible to obtain both QM and CM solutions. But the harmonic approximation is not valid in the most interesting regime when more complex molecular motions appear due to the anharmonicity of the real potential. On the other hand, MD and MC simulations allow to take into account the anharmonicity of the real potential. Thus it would be valuable to find a way to correct the results of the CM calculation in such a way that at very low temperatures the corrected results would reproduce the results of low temperature QM calculations, while at high temperatures they would track the anharmonicity of the real potential.

Consider the following expression:

$$\sigma^2(T) = \sigma_{CM}^2(T) + [\sigma_{HQM}^2(T) - \sigma_{HCM}^2(T)], \quad (4.31)$$

where under $\sigma_{CM}^2(T)$ we mean the CM results on some potential $U(x)$ that could be obtained from the Monte Carlo or Molecular Dynamics simulations and thus sensitive to the anharmonicity of the real potential. Under $\sigma_{HQM}^2(T)$ we mean the QM solution for the harmonic approximation to $U(x)$ in the vicinity of r_o . Finally $\sigma_{HCM}^2(T)$ stands for the CM solution for the harmonic approximation to $U(x)$. At very low temperatures, $\sigma^2(T) = \sigma_{HQM}^2(T)$, since $\sigma_{CM}^2(T) \simeq 0$ for the both potentials. As the temperature increases, see Fig.4.4, the difference of the two terms in square brackets in (4.31) decreases and thus becomes: $\sigma^2(T) \simeq \sigma_{CM}^2(T)$. Thus, the form (4.31) reproduces the correct behavior of the *real* $\sigma^2(T)$. It follows from Fig.4.4 that results that were obtained using CM on the Morse potential, and corrected by (4.31), the corrections that comes from the harmonic approximation to the Morse potential reproduce the exact QM solution to the Morse potential in the whole range of the reasonable

temperatures rather well.

In general the line shape of the PDF for a pair of atoms obtained in MD or MC simulations is not Gaussian. Thus the correction (4.31) could not be applied directly in order to correct (4.3) since the σ_{ij}^2 are not known. It is known that:

$$\begin{aligned} \int_{-\infty}^{\infty} \frac{1}{\sqrt{2\pi\sigma_1^2}} \exp\left[-\frac{(r-r')^2}{2\sigma_1^2}\right] \frac{1}{\sqrt{2\pi\sigma_2^2}} \exp\left[-\frac{(r_o-r')^2}{2\sigma_2^2}\right] dr' \\ = \frac{1}{\sqrt{2\pi(\sigma_1^2 + \sigma_2^2)}} \exp\left[-\frac{(r-r_o)^2}{2(\sigma_1^2 + \sigma_2^2)}\right]. \end{aligned} \quad (4.32)$$

Thus, the convolution (4.32) of one Gaussian with another increases the width of the original Gaussian. If instead of one Gaussian another function that has some peak in it would be used, then the convolution still would increase the width of the peak, while the height would decrease.

In MC or MD simulations, the distance between a pair of atoms would oscillate around some average value, at low enough temperatures. Thus, the PDF obtained from MC or MD simulations would represent some distribution with a peak. Thus the correction (4.31) still can be applied by the convolution:

$$G(r) = \int G_{MD}(r') \frac{1}{\sqrt{2\pi\sigma_{corr}^2}} \exp\left[-\frac{(r-r')^2}{2\sigma_{corr}^2}\right] dr' . \quad (4.33)$$

where *the correction width* is given by:

$$\sigma_{corr}^2(T) = [\sigma_{HQM}^2(T) - \sigma_{HCM}^2(T)]. \quad (4.34)$$

In (4.33, 4.34) $G_{MD}(r')$ stands for the PDF (distribution of distances) of the atomic pair obtained from the MC or MD simulations and $G(r)$ stands for the corrected PDF. The weighted sum over the different pairs leads to the corrected PDF (4.3). The black dashed curves on Fig.4.3 show the CM results on the Morse potential (4.13,4.14) corrected by the convolution (4.33,4.34).

4.3.2 Correction to the heat capacitance

The same philosophy that was used to correct $\sigma^2(T)$ could be used to correct the classically calculated heat capacitance. According to QM, the average value of the *total* energy of an oscillator (a diatomic molecule) in a potential (Morse or Harmonic) could be found as:

$$\langle E_{QM}(T) \rangle = \frac{1}{Z_{QM}} \sum_{n=0}^{n_{max}} E_n \exp\left[-\frac{E_n}{k_b T}\right], \quad (4.35)$$

where Z_{QM} is given by (4.25).

In the classical approach, the average value of the total energy could be found as the sum of the average values of kinetic and potential energies:

$$\langle E_{CM}(T) \rangle = \langle K(T) \rangle + \langle U(T) \rangle. \quad (4.36)$$

The value of the kinetic energy at temperature T is given by [64]:

$$\langle K(T) \rangle = \frac{1}{2} k_b T, \quad (4.37)$$

while the average value of the potential energy could be found as [64]:

$$\langle U(T) \rangle = \frac{1}{Z_{CM}} \int U(x) \exp\left[-\frac{U(x)}{k_b T}\right] dx, \quad (4.38)$$

where Z_{CM} is given by (4.14). See Appendix (B) on the integration range.

If the average value of the total energy for a diatomic molecule is known as a function of temperature, then the vibrational heat capacitance could be found as:

$$C(T) = \frac{dE(T)}{dT}. \quad (4.39)$$

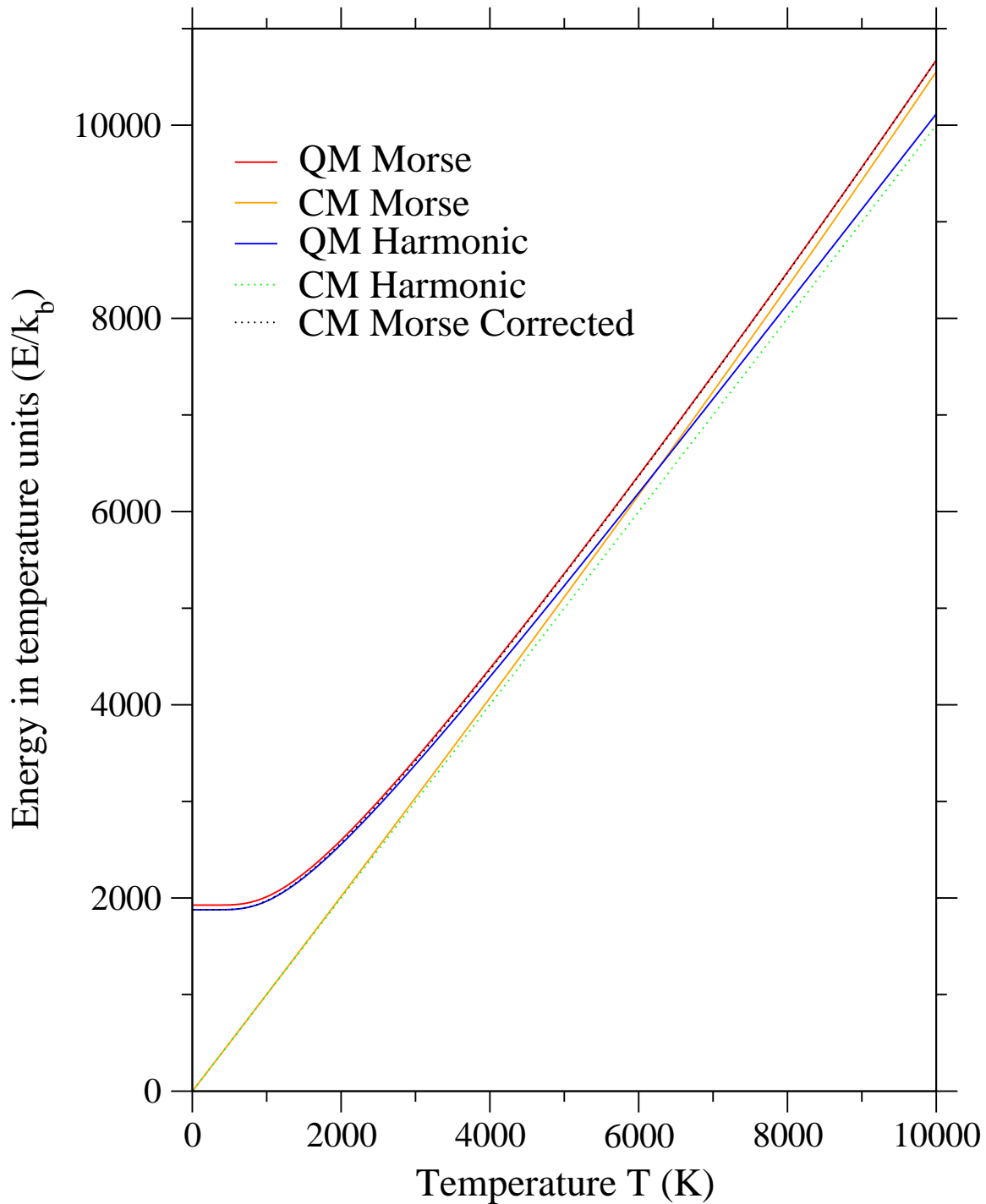


Figure 4.5: Average energies for a particle in the Morse potential and its harmonic approximation as a function of temperature. The red and orange curves represent the QM and CM solution for the Morse potential. The blue and green (dashed) curves show the QM and CM solutions for the harmonic approximation to the Morse potential. The black dashed curve shows the CM solution for the Morse potential with correction (4.31) that comes from the harmonic approximation to the Morse potential. It is assumed that $U_o = 0$.

Figure 4.5 shows the dependence of the total average energy for a particle in the Morse and Harmonic potentials. The values of parameters are the same that were used to obtain Fig.4.4. The red and orange curves were calculated via the QM (4.35,4.25) and CM (4.36,4.37,4.38) for the Morse potential. The blue (QM) and green (CM) curves were calculated for the harmonic approximation to the Morse potential.

Again, as we did in (4.31), we can consider the correction of the CM results for the Morse potential by using the results from the harmonic approximation to the Morse potential:

$$E(T) = E_{MCM}(T) + [E_{HQM}(T) - E_{HCM}(T)]. \quad (4.40)$$

The fact that the corrected curve is very close to the exact QM solution obtained on the Morse potential shows that this correction method also works well for the average energy in a wide range of temperatures.

The heat capacitance can be obtained by the differentiation (4.39) of the energy curves. Figure 4.6 shows how the heat capacitances found by the differentiation of the energy curves on Fig.4.5 depend on temperature.

Since in the harmonic potential, the average values of the kinetic and potential energies are the same and due to (4.37) the classical heat capacitance for the particle in the harmonic potential is just k_b or unity in units used on Fig.4.6. The behavior of the QM solution for the harmonic potential is also well known [64]. Thus, we can see that our correction method again leads to a very good agreement between the approximate (corrected) and the exact (QM Morse) results.

4.4 Vibrations of large molecules

Let us assume initially that atoms in the molecule vibrate near their equilibrium positions with amplitudes of vibrations that are much smaller than any interatomic

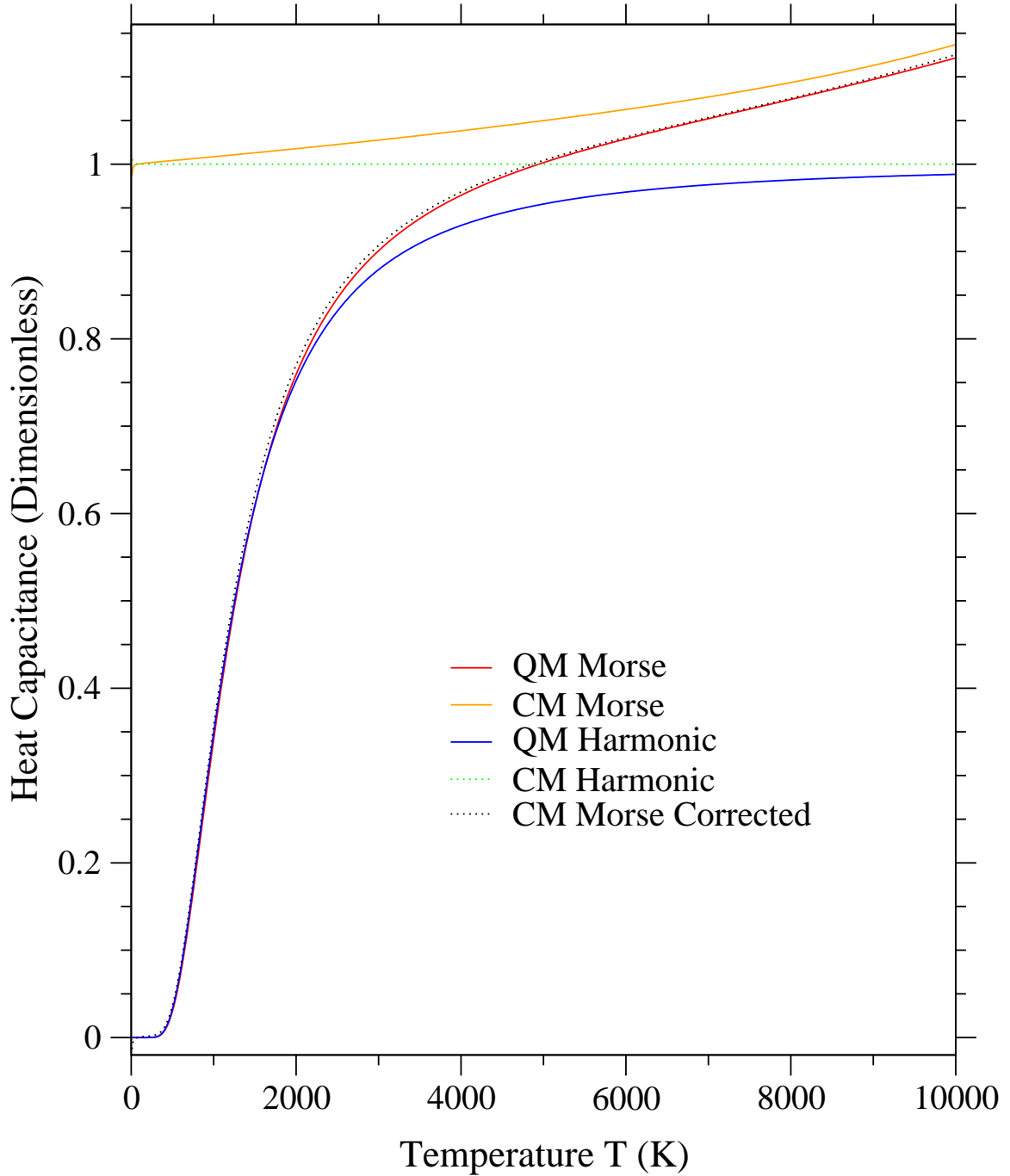


Figure 4.6: The dependencies of the heat capacitances for the particle in the Morse potential and its harmonic approximation on temperature. The red and orange curves represent QM and CM solutions for the Morse potential. The blue and green (dashed) curves show the QM and CM solutions for the harmonic approximation to the Morse potential. The black dashed curve shows the CM solution for the Morse potential with the correction (4.31) that comes from the harmonic approximation to the Morse potential. All these curves were obtained by the differentiation (4.39) of the corresponding energy curves on Fig.4.5.

distances. Thus for the moment we ignore the possibility of the large-scale atomic motion that can be caused by the flexibility of the molecule. In order to calculate the PDF it is necessary to calculate the mean square deviations of the distances between the atoms from their equilibrium values: σ_{ij}^2 . Let the coordinates of atoms i and j be $\vec{r}_i = \vec{r}_i^o + \vec{u}_i$ and $\vec{r}_j = \vec{r}_j^o + \vec{u}_j$, where \vec{r}_i^o and \vec{r}_j^o are the equilibrium coordinates of atoms i and j , while their instantaneous displacements are \vec{u}_i and \vec{u}_j . Let also: $\vec{r}_{ij} = \vec{r}_j - \vec{r}_i$, $\vec{r}_{ij}^o = \vec{r}_j^o - \vec{r}_i^o$ and $\vec{u}_{ij} = \vec{u}_j - \vec{u}_i$. Then it is easy to show, under the assumption $u_{ij} \ll r_{ij}^o$, that:

$$\begin{aligned} \sigma_{ij}^2 &= \langle (r_{ij} - r_{ij}^o)^2 \rangle \cong \langle [\hat{r}_{ij}^o \vec{u}_{ij}]^2 \rangle \\ &= \sum_{\alpha, \beta} \hat{r}_{ij}^{o\alpha} \hat{r}_{ij}^{o\beta} \langle (u_{i\alpha} u_{j\beta} - u_{i\alpha} u_{j\beta} - u_{j\alpha} u_{i\beta} + u_{j\alpha} u_{j\beta}) \rangle \end{aligned} \quad (4.41)$$

where $\hat{r}_{ij}^o = \vec{r}_{ij}^o / r_{ij}^o$. The indexes α, β stand for the Cartesian coordinates of the vectors.

We consider here the vibrations of a molecule that consists of N atoms with masses m_i . The potential energy of the molecule $U(\vec{x})$ is a function of the coordinates \vec{x} of all the atoms. There are $3N$ components x_i of the vector \vec{x} . Thus the index i runs over all the atoms and over all their Cartesian coordinates.

Let us assume that the atoms vibrate near their equilibrium positions \vec{x}_o and that their instantaneous coordinates are $\vec{x} = \vec{x}_o + \vec{u}$. If vector \vec{u} is small enough the potential energy could be expanded near the equilibrium (\vec{x}_o):

$$U(x) \cong U_o + \frac{1}{2} \sum_{ij} D_{ij} u_i u_j, \quad (4.42)$$

where

$$D_{ij} = \frac{\partial^2 U(\vec{x}_o)}{\partial x_i \partial x_j} \quad (4.43)$$

is a real symmetric matrix. Thus for the Hamiltonian we have:

$$H = \sum_i \frac{p_i^2}{2m_i} + \frac{1}{2} \sum_{ij} D_{ij} u_i u_j. \quad (4.44)$$

It is convenient to introduce new variables

$$p_i = \sqrt{m_i} \pi_i, \quad u_i = q_i / \sqrt{m_i} \quad (4.45)$$

that will transform (4.44) into:

$$H = \sum_i \frac{\pi_i^2}{2} + \frac{1}{2} \sum_{ij} \tilde{D}_{ij} q_i q_j, \quad (4.46)$$

where $\tilde{D}_{ij} = D_{ij} / \sqrt{m_i m_j}$.

Since \tilde{D}_{ij} is a real and symmetric matrix it could be brought to the diagonal form by the linear transformations of q_i :

$$q_i = \sum_{\lambda} e_i^{\lambda} Q_{\lambda}, \quad (4.47)$$

where \bar{e}^{λ} could be chosen as real, orthogonal and normalized:

$$\sum_i e_i^{\lambda} e_i^{\lambda'} = \delta_{\lambda\lambda'}. \quad (4.48)$$

In this case the transformation:

$$\pi_i = \sum_{\lambda} e_i^{\lambda} P_{\lambda} \quad (4.49)$$

will also bring to the diagonal form the first sum in (4.46). Thus we can rewrite

Hamiltonian as:

$$H = \sum_{\lambda} \frac{1}{2} [P_{\lambda}^2 + \omega_{\lambda}^2 Q_{\lambda}^2]. \quad (4.50)$$

The second quantization:

$$Q_{\lambda} = \frac{1}{2} \sqrt{\frac{\hbar}{\omega_{\lambda}}} (a_{\lambda}^{\dagger} + a_{\lambda}), \quad P_{\lambda} = \frac{i}{2} \sqrt{\hbar \omega_{\lambda}} (a_{\lambda}^{\dagger} - a_{\lambda}), \quad (4.51)$$

with $[P, Q] = i\hbar$ so that $a_{\lambda}^{\dagger} a_{\lambda'} - a_{\lambda'} a_{\lambda}^{\dagger} = \delta_{\lambda\lambda'}$ transforms (4.50) into:

$$H = \sum_{\lambda} \hbar \omega_{\lambda} (a_{\lambda}^{\dagger} a_{\lambda} + \frac{1}{2}) \quad (4.52)$$

as it should. Thus $\langle \psi | H | \psi \rangle = \sum_{\lambda} \hbar \omega_{\lambda} (n + 1/2)$.

From (4.45,4.47,4.51) follows that:

$$u_i = \sum_{\lambda} e_i^{\lambda} \sqrt{\frac{\hbar}{2m_i \omega_{\lambda}}} (a_{\lambda}^{\dagger} + a_{\lambda}). \quad (4.53)$$

Thus, separating the atomic and Cartesian coordinates, we get:

$$\langle \psi | u_{i\alpha} u_{j\beta} | \psi \rangle = \sum_{\lambda} \frac{\hbar}{2\omega_{\lambda}} (n_{\lambda} + \frac{1}{2}) \frac{e_{i\alpha}^{\lambda}}{\sqrt{m_i}} \frac{e_{j\beta}^{\lambda}}{\sqrt{m_j}}. \quad (4.54)$$

It is easy to show, using (4.54), that (4.42) transforms into:

$$\sigma_{ij}^2 = \sum_{\lambda} \frac{\hbar}{2\omega_{\lambda}} [n_{\lambda} + \frac{1}{2}] \left\{ \frac{(\vec{e}_i^{\lambda} \hat{r}_{ij}^o)}{\sqrt{m_i}} - \frac{(\vec{e}_j^{\lambda} \hat{r}_{ij}^o)}{\sqrt{m_j}} \right\}^2, \quad (4.55)$$

where n_{λ} is the Bose-Einstein function (4.10) that at high temperatures can be substituted by (4.11). It is easy to see that (4.55) in case of the diatomic molecules ($m_1 = m_2 = m$) reduces to (4.9), if to take into account that $\mu = m/2$ and $(\vec{e}_i \hat{r}_{ij}) - (\vec{e}_j \hat{r}_{ij}) = 2$.

MD or MC simulations at low temperatures, when the anharmonicity of the real potential can be ignored, would lead to (4.55, 4.11), while the correct result is (4.55, 4.10). It is clear from (4.7, 4.9, 4.10, 4.11, 4.12) and from (4.52, 4.55) that the formulas (4.31, 4.40) used to correct the CM results in case of the diatomic molecule can be modified in an obvious way in order to correct the CM results that were obtained on a many-atomic molecule, i.e.:

$$E(T) = E_{CM}(T) + \sum_{\lambda} [E_{HQM}(\lambda, T) - E_{HCM}(\lambda, T)]. \quad (4.56)$$

The width of the peaks can be corrected via

$$\sigma^2(T) = \sigma_{CM}^2(T) + \sigma_{corr}^2(T), \quad (4.57)$$

where

$$\sigma_{corr}^2(T) = \sum_{\lambda} [\sigma_{HQM}^2(\lambda, T) - \sigma_{HCM}^2(\lambda, T)] \quad (4.58)$$

and the index λ runs over different vibrational modes.

From the result of MD or MC calculation only the total (not for the particular vibrational mode) average values of the $E_{CM}(T)$ and $\sigma_{CM}^2(T)$ could be found.

4.5 TINKER package for molecular modelling and the C_6H_{14} molecule

In order to demonstrate the role of the quantum corrections (4.56, 4.57) for a more complicated molecule, it is necessary to find the eigenfrequencies and eigenvectors of molecular vibrations as well as the results of the classical MD or MC simulations.

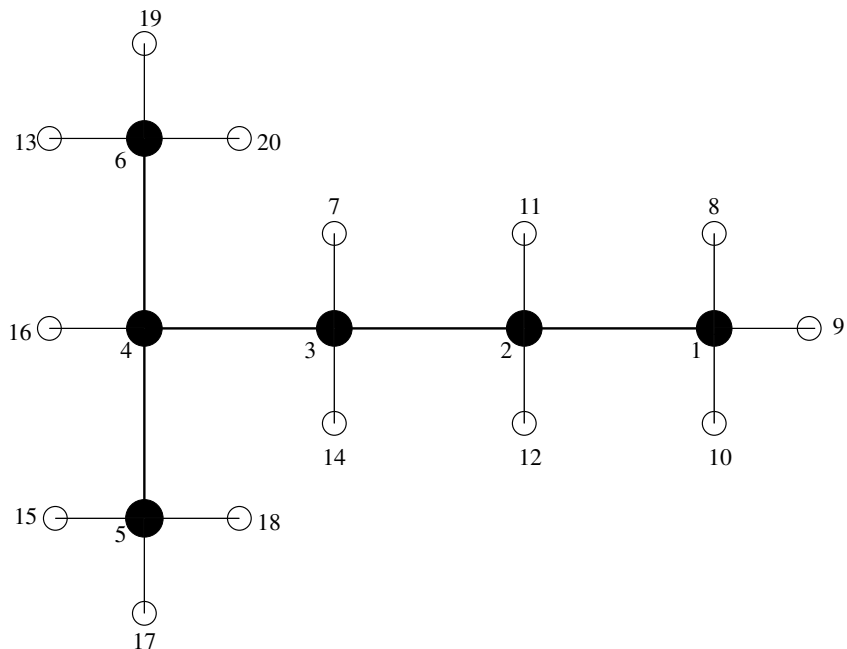


Figure 4.7: The sketch of the C_6H_{14} molecule. The carbon atoms are shown as black filled circles. The hydrogen atoms are shown as open circles. The numeration of the atoms coincides with those used in the Fig.4.9 and Fig. 4.10.

There are many different potentials and programs developed for the different kinds of molecules. One of the most developed potentials are those developed for hydrocarbons. One of them is the so called “MM3” potential [66, 67, 68, 69, 70, 71, 72, 73]. One of the programs (a package that includes several different programs) that can use this potential to optimize the molecular structure, calculate the eigenfrequencies (ω_λ) and eigenvectors (\vec{e}^λ) in a particular equilibrium configuration and to run MD at given temperature is “TINKER” [74, 75, 76, 77, 78, 79, 80]. As an output of MD simulations (for a single molecule) at given temperature, TINKER provides the coordinates of the atoms, the total energy, the kinetic and potential energies as functions of time.

We use the C_6H_{14} - molecule as a test example. Figure 4.7 shows the sketch of the C_6H_{14} molecule, while the Fig.4.8 shows the geometry of the C_6H_{14} molecule in *Long* conformation. At room temperature the C_6H_{14} molecule is relatively flexible,

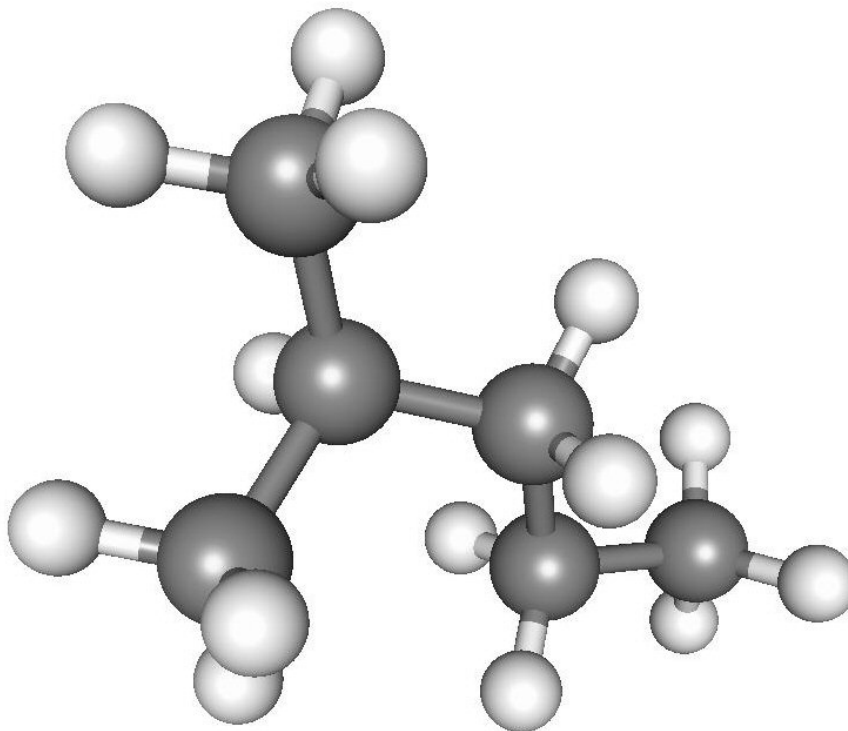


Figure 4.8: The geometry of the C_6H_{14} molecule in *Long* conformation.

as we will see. At normal pressure these molecules form a non-toxic and not very flammable liquid and thus its PDF can be easily measured.

At low temperatures the C_6H_{14} molecule can be in two different conformations, as follows from MD simulations and structures optimizations with TINKER, which we call *Long* and *Short*. The distances between some atoms in these molecular conformations are shown in the table 4.1. The ground state tension energies (obtained from

Pair of Atoms $i - j$	1 - 4	1 - 5	1 - 6
Distance between i and j (<i>Long</i>), (Å)	3.94	4.56	5.07
Distance between i and j (<i>Short</i>), (Å)	3.17	4.54	3.81

Table 4.1: The distances between some atoms in *Long* and *Short* conformations.

TINKER) of the molecule in *Long* and *Short* conformations are slightly different:

$$E_L = 6.3479 \text{ (kcal/mol)}, \quad (4.59)$$

$$E_S = 7.1293 \text{ (kcal/mol)},$$

where L stands for the *Long* and S for the *Short*. The difference in the energies between these two conformations per molecule in temperature units is:

$$\Delta E = E_S - E_L \approx 393 \text{ (K)}. \quad (4.60)$$

4.6 Calculation of PDF for C_6H_{14} molecule

4.6.1 Low temperatures

The blue curves on Fig.4.9 show the probabilities for finding the pairs of atoms 1-2, 1-3, 1-4, 1-5, 1-6 at a given distance obtained from MD simulations at temperatures 150 K and 500 K. In the beginning of MD runs, the molecule was always in an equilibrium *Long* conformation. At temperature 150 K the molecule remains in *Long* conformations during the MD run. At temperature 500K the molecule continuously switches between different conformations (it is flexible). The time step in MD simulations was $\Delta t = 1$ femtoseconds. The coordinates of the atoms were saved after every 1000 MD time steps. The blue curves represent the distributions obtained from 10,000 different molecular configurations. Thus the total run time was 10,000 picoseconds. The red curves were obtained by the convolution (4.33,4.34) of the blue curves with the Gaussian whose correction width σ_{corr} that corresponds to the given pair of atoms for the molecule is in *Long* conformation.

At low temperature, when the molecule is frozen in the *Long* or *Short* configuration, atoms only vibrate slightly near their equilibrium positions. As the temperature

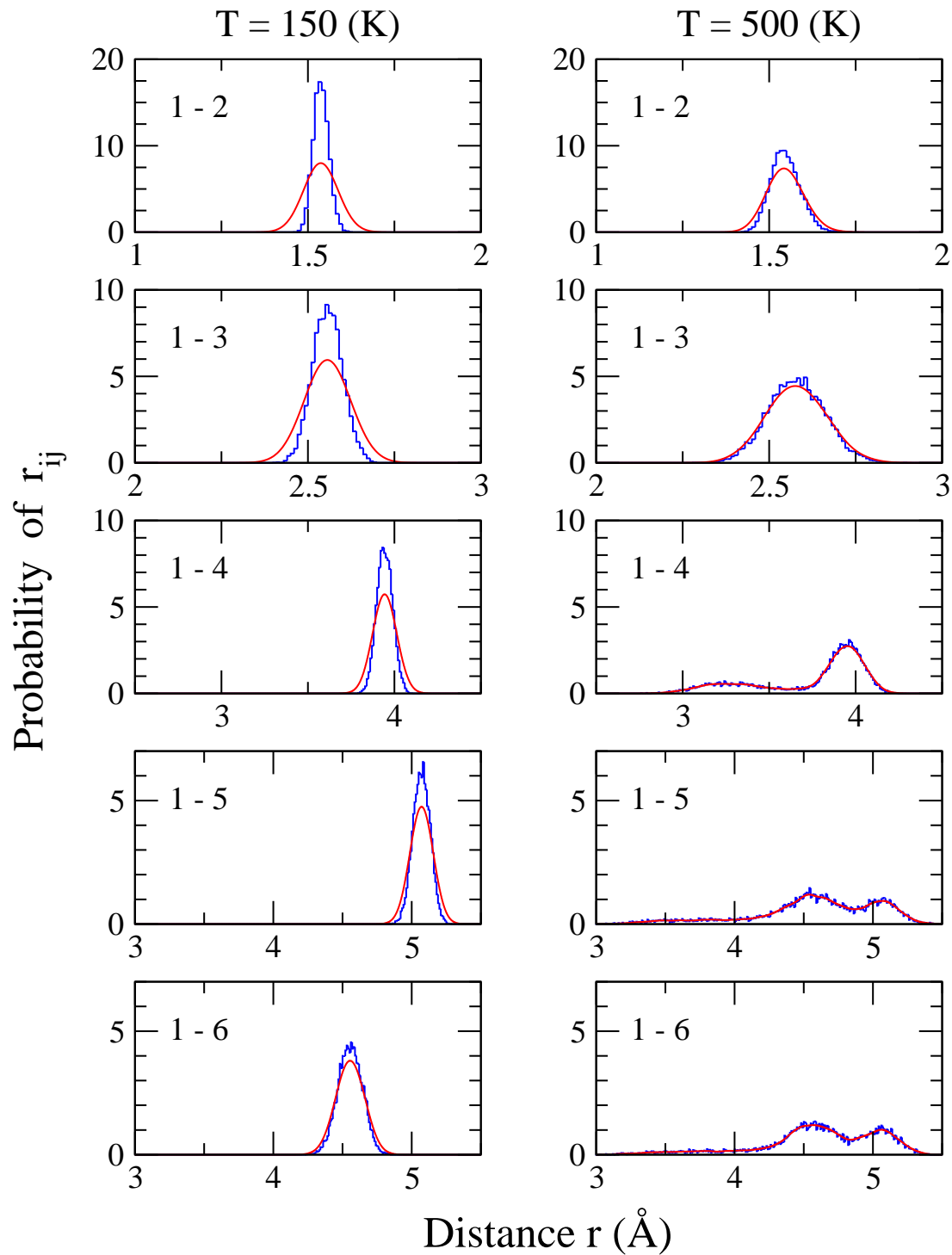


Figure 4.9: The probability for finding a particular pair of atoms at a given distance at temperatures 150K on the left and at 500K on the right. The blue curves were obtained from the classical MD trajectories. The red curves result from the convolution of the blue curves with the corresponding correction Gaussian. Every pair of the atoms has its own $\sigma_{corr}^2(T)$.

increases, there can occur transitions between *Long* and *Short* configurations. This behavior could be seen from the change in the peak shape for the pairs of atoms 1-4, 1-5, 1-6 when temperature changed from 150 K to 500 K. At 150 K those peaks are relatively narrow and symmetric, while at 500 K the peaks become much broader and their shape indicates that there are two conformations in which the molecule spends most of its time.

If the molecule during the MD run remains all the time in *Long* or *Short* conformation it is clear what set of the correction σ_{corr} should be used. If the molecule changes its conformation during the MD run, it becomes unclear what σ_{corr} set should be used: from *Long* or from *Short* conformation. We will discuss this issue later.

The orange triangles on the Fig.4.10 show how the σ_{CM}^2 obtained in MD runs depend on temperature. The blue and green curves show $\sigma^2(T)$ that were obtained in the harmonic approximation from the eigenfrequencies and eigenvectors of molecular vibrations in the frame of QM (4.55,4.11) and CM (4.55,4.10) respectively. The red circles were obtained by applying the correction (4.57) to the MD results. Thus at very low temperatures the results of MD simulations agree with the CM results obtained in the harmonic approximation, as it should be. However the correct results at these temperatures are given by the QM results on the harmonic potential (the blue curve). Thus our correction, if applied, shifts the orange triangles into the red circles that fit QM results at low temperatures very well. As temperature increases the anharmonicity of the potential usually makes potential softer, thus increasing $\sigma^2(T)$ compared with the harmonic case. The sharp increase in the $\sigma^2(T)$ with increase of temperature that occurs for some pairs of atoms corresponds to the appearance of flexibility. Thus the molecule becomes flexible between 200 and 300 K. It is easy to see, from the numbers of the atoms, that it is the dihedral angles that become flexible.

If the molecular trajectory is known the PDF (4.3) could be found if the distributions of lengths (the blue curves on Fig.4.9) for every pair of atoms will be used

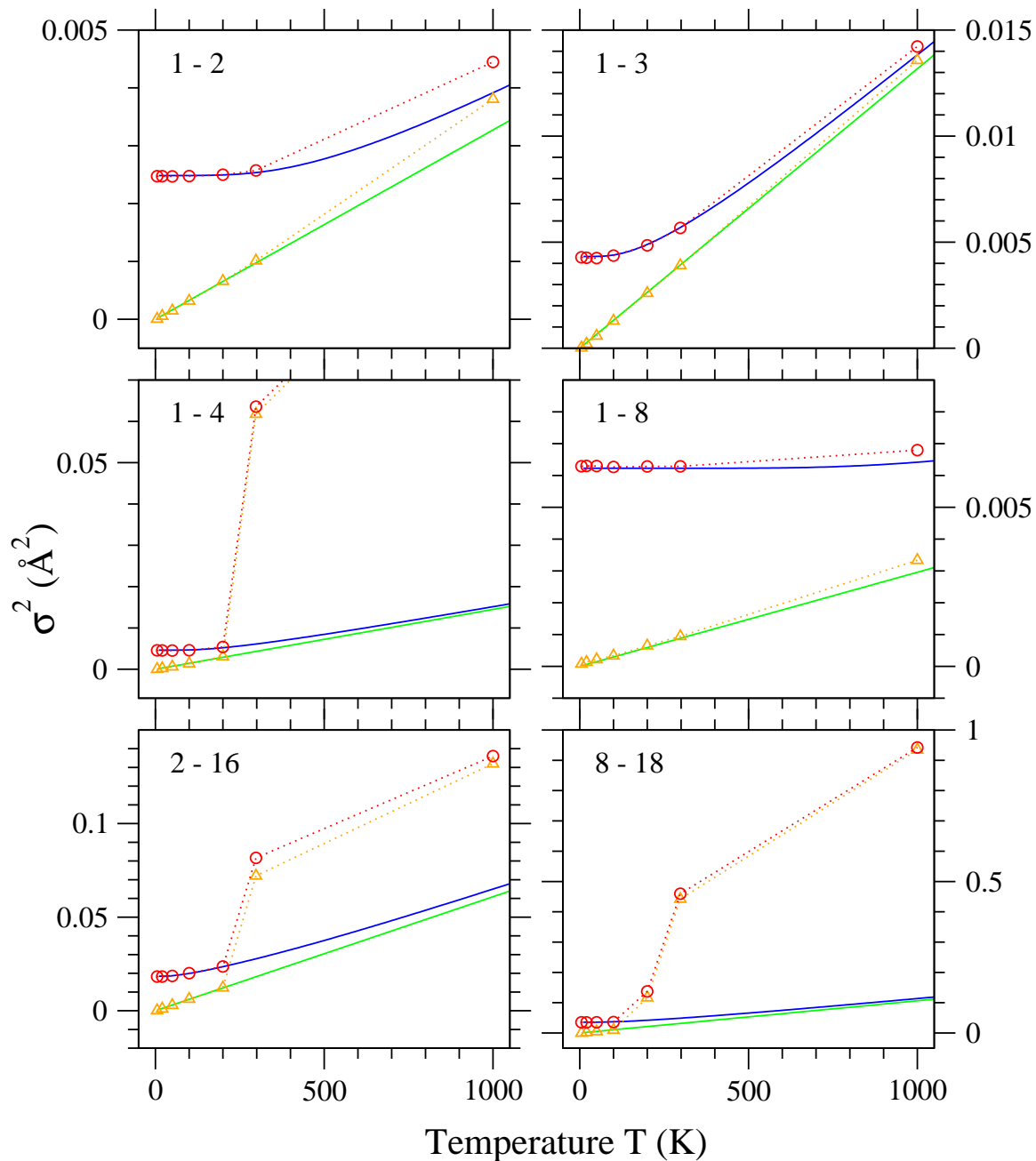


Figure 4.10: The dependencies of σ^2 on temperature T for some pairs of atoms. The orange triangles show the results obtained from MD simulations, the blue and green curves show the QM and CM results obtained from the eigenfrequencies and eigenvectors of molecular vibrations. The red circles show the MD results corrected by adding to the orange triangles the difference between the blue and green curves.

instead of the Gaussians in (4.3). The correction could be made by the convolution of the distribution of distances for every pair of atoms with the gaussians (4.33,4.34). The brown curves on the Fig.4.11 show the PDFs obtained in MD simulations when the molecule remains in *Long* conformation before the correction, while the blue curves show the corrected PDFs. Thus at low temperatures the correction significantly changes the shape of the PDF. The role of the correction remains important at small distances at all temperatures, while at large distances its role decreases as temperature increases because the widths of peaks that correspond to the atoms that are well separated become significantly larger in MD simulations.

It is not known in general how many molecules are in a particular conformation. The relative contributions of different conformations to the total PDF depend on the shape of the free energy surface. Since the line shape of the free energy is not known the simplest way to combine the results obtained on different conformations is to assign the Boltzman weights to the PDFs in different conformations. Thus the weight for the molecule in *Long* conformation:

$$w_L(T) \propto \exp\left[-\frac{E_L}{k_b T}\right], \quad (4.61)$$

Thus for the C_6H_{14} molecule at low temperatures the total PDF can be calculated as a linear combination of the PDFs from *Long* and *Short* conformations with the corresponding Boltzman weights.

$$G(r, T) = w_L(T)G_L(r, T) + w_S(T)G_S(r, T), \quad (4.62)$$

where $G_L(r, T)$ and $G_S(r, T)$ are the corrected PDFs from *Long* and *Short* conformations. The Boltzman weights $w_L(T)$ and $w_S(T)$ are given by:

$$w_L(T) = \frac{1}{1 + \exp\left[-\frac{\Delta E}{k_b T}\right]} \quad (4.63)$$

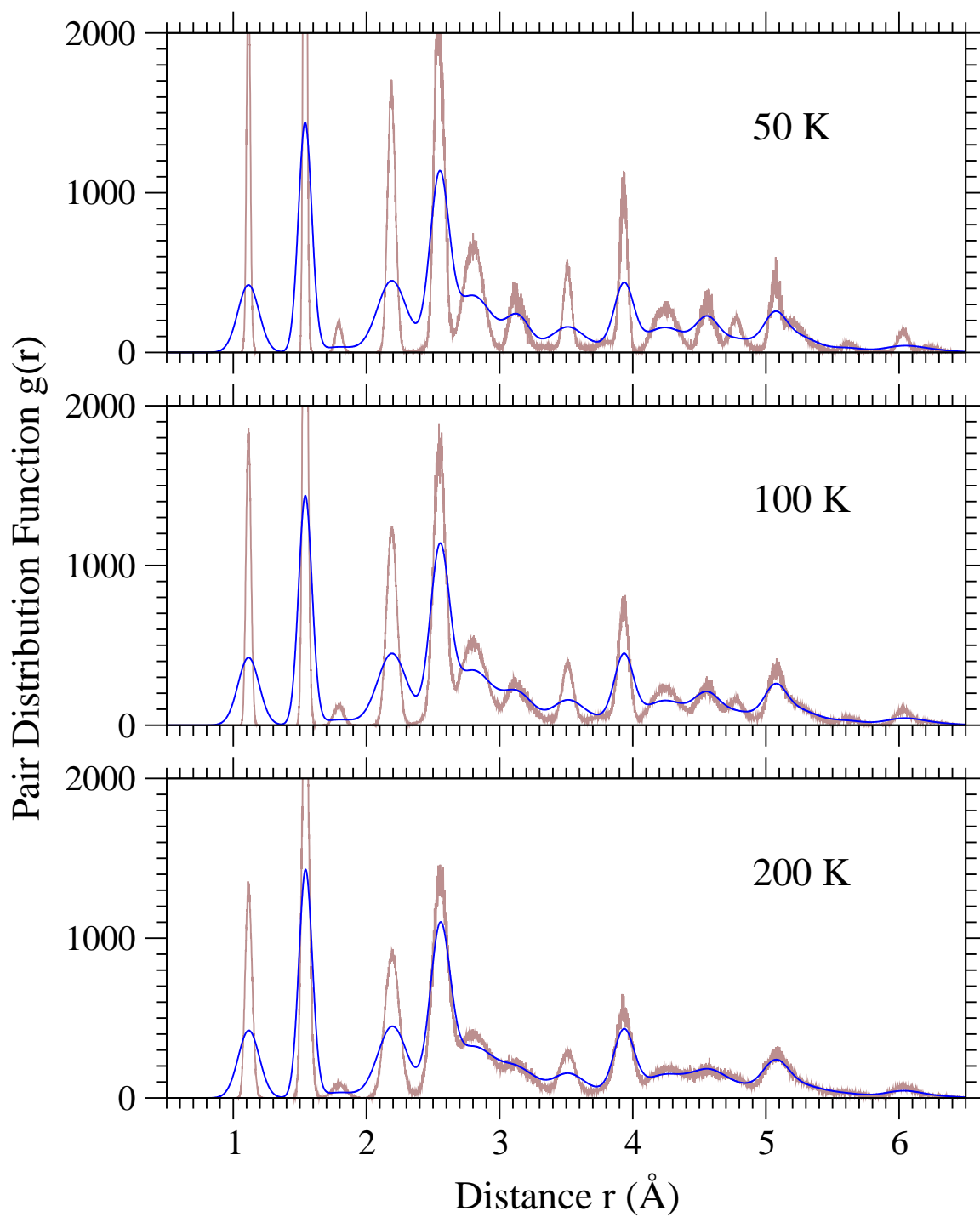


Figure 4.11: PDF for the C_6H_{14} molecule in *Long* conformation at low temperatures. The brown curves show the results of MD simulations before the correction is applied. The blue curves show the results of MD simulations corrected by convolution (4.33, 4.34).

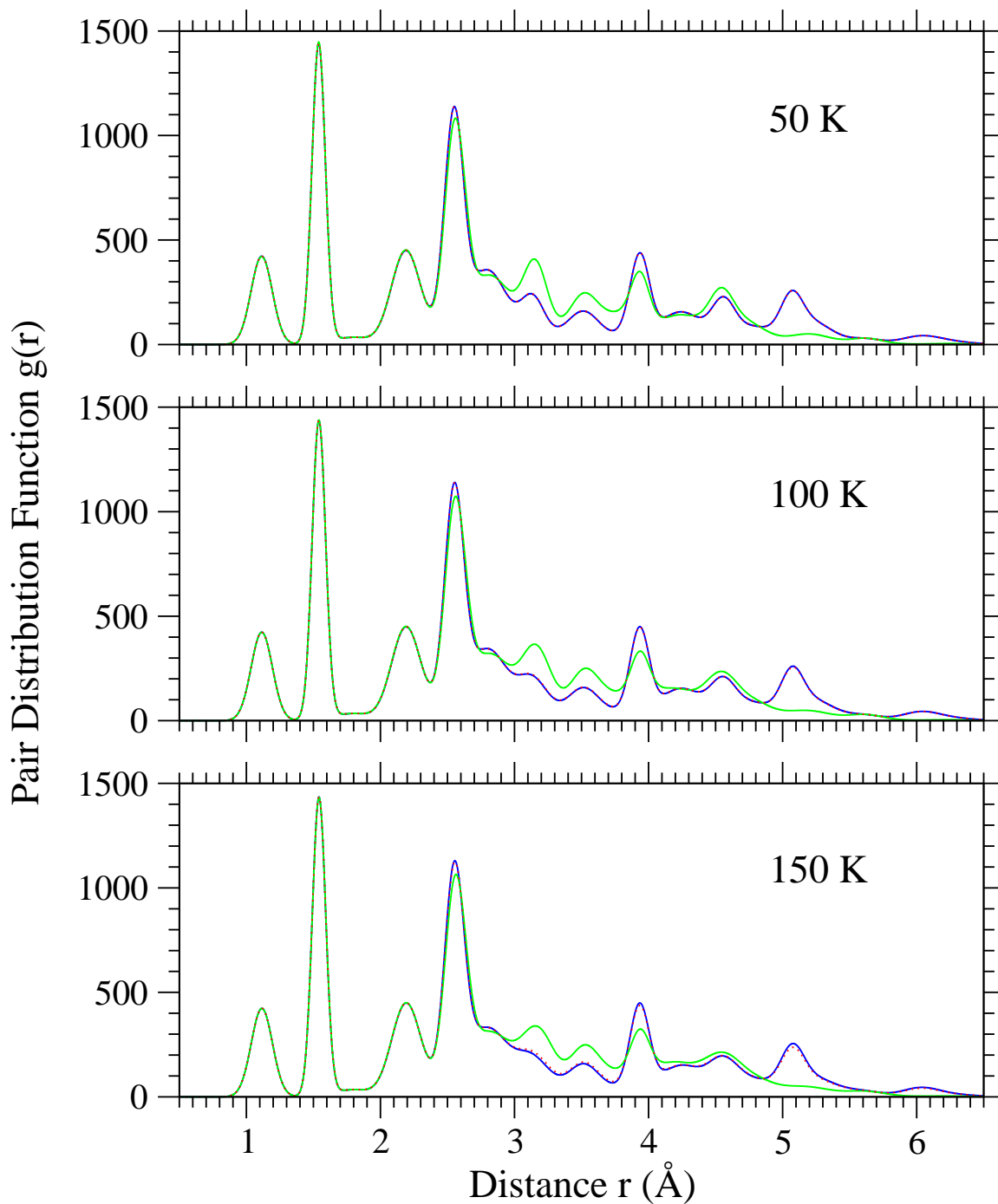


Figure 4.12: The blue and green solid curves show total corrected PDFs for the molecule in *Long* and *Short* conformations. The red dashed curve shows Boltzman combination (4.62) of PDFs from *Long* and *Short* conformations. At all temperatures when the molecules remains in one or another conformation the combined PDF basically coincides with PDF in *Long* conformation due to the values of the Boltzman weights.

and

$$w_S(T) = \frac{\exp\left[-\frac{\Delta E}{k_b T}\right]}{1 + \exp\left[-\frac{\Delta E}{k_b T}\right]}. \quad (4.64)$$

so that: $w_L(T) + w_S(T) = 1$. Table 4.2 shows $w_L(T)$ and $w_S(T)$ for temperatures 50, 100, 150, 200 (K).

Temperature T (K)	50	100	150	200
$w_L(T)$	0.9997	0.98	0.91	0.85
$w_S(T)$	0.0003	0.02	0.09	0.15

Table 4.2: Boltzman weights for C_6H_{14} molecule in *Long* and *Short* conformations at different temperatures.

The corrected PDFs for the C_6H_{14} molecule in *Long* and *Short* conformations at different temperatures are shown in Fig.4.12 as the blue and green curves respectively. The red curves in Fig.4.12 show PDFs calculated according to (4.62) with the Boltzman weights taken from the table 4.2.

4.6.2 High temperatures

In order to use the Boltzman combination of the PDFs in different conformations to obtain the total combined PDF, the molecule should remain in one or the other conformation during the MD run, or it is necessary to separate those times (parts of the molecular trajectory) when the molecule is in one or in the other conformation. It is necessary to do this because every conformation has its own set of σ_{corr} that was obtained using the eigenfrequencies and eigenvectors of the molecular vibrations in the corresponding conformation.

In practice, however, it is impossible to say when the molecule is in one or in the other conformation. For example even when the molecule remains in *Long* or *Short* conformation the positions of atoms 8 and 9 can interchange during the MD run. When it happens the molecule is already in a different conformation since atoms

8 and 9 have different sets of σ_{corr} with respect to the other atoms. Thus although the geometry of the molecule did not change during the interchange of positions of atoms 8 and 9, the sets of σ_{corr} should be modified. It seems to be an impossible task to track all such little changes. Another reason that does not allow separation of different conformations at high temperatures comes from the observation that the changes in the distances between some pairs of atoms, due to the vibrations, become comparable with the changes in the distances caused by the changes in the conformations. Thus basically it becomes impossible to say when the molecule is in one or in the other conformation. Thus, at high temperatures, the approach that combines PDFs in different conformations with the corresponding Boltzman weights becomes unacceptable.

Instead another approach could be used. In order to obtain the corrected PDF in *Long* conformation it is necessary to convolute the PDF obtained from the MD trajectory in *Long* conformation with the set of σ_{corr} that was also obtained on the *Long* conformation. Assume that instead of convolution performed with the set of σ_{corr} from the *Long* conformation we will use the set of σ_{corr} from the *Short* conformation. How different would the corrected PDFs be when obtained with these two different sets of σ_{corr} from the same MD trajectory?

The brown curves on Fig.4.13 show PDFs obtained from the MD trajectory at temperature 50 K when the molecule remains in the *Long* (top) or in the *Short* (bottom) conformation depending on initial configuration. The blue solid curve originates from the convolutions of the MD results from the *Long/Short* conformations with the correct sets of σ_{corr} from the *Long/Short* conformations. The red dashed curves were obtained by the convolution of the brown curves with the incorrect sets of σ_{corr} : the MD results from the *Long/Short* conformations were convoluted with the σ_{corr} from the *Short/Long* conformations.

Thus we see that although there are very significant differences between the

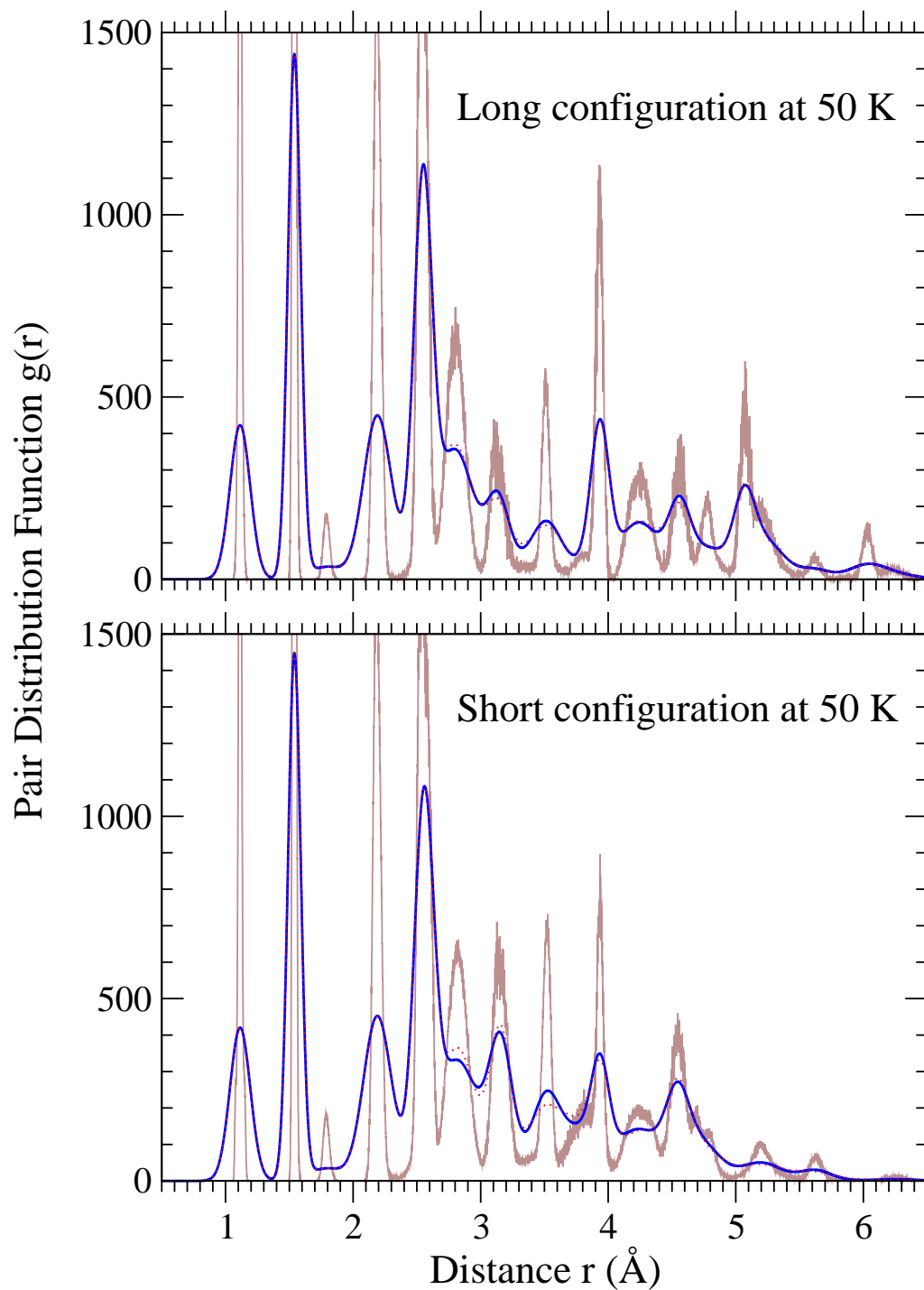


Figure 4.13: The brown curves on both figures show MD results obtained on the *Long* (top) and *Short* (bottom) conformations. The figure on top also shows the corrected PDFs obtained by the correction of MD results from the *Long* conformation with the set of σ_{corr} from the *Long* (the blue solid curve) and *Short* (the red dashed curve) conformations. The bottom figure also shows the PDFs obtained by the correction of MD results from the *Short* conformation with the sets of σ_{corr} from *Short* (blue solid curve) and *Long* (red dashed curve) conformations.

non-convoluted and convoluted (corrected) PDFs the differences between the PDFs obtained by the convolutions with different sets of σ_{corr} are rather small.

The small differences between the MD results corrected with the different sets of σ_{corr} could be easily understood. Our correction is the most significant (large σ_{corr}) for those pairs of atoms that are tightly connected, i.e. by a bond or by an angle. Thus the correction is significant for those atoms that are close to each other. The mutual vibrations of such pairs (distance distribution) are slightly affected by the general conformation of the molecule—they are almost the same for all of them. On the other hand, if atoms in a pair are far away from each other then the corresponding σ_{corr} are small in general, independently from the molecular configuration. Thus the correction is not that important for those pairs in principle. That means that in order to apply the correction we can convolute the PDF obtained from the MD simulations with a set of σ_{corr} from any particular configuration. At higher temperatures the differences between the curves obtained by convolutions with different sets of $\sigma_{corr}(T)$ will become even smaller since $\sigma_{corr}(T)$ decrease with increase of temperature (see Fig.4.4,4.10).

Figure 4.14 show PDFs calculated for the C_6H_{14} molecule at different temperatures. The PDFs at temperatures 50 (K) and 150 (K) were obtained by combining the PDFs from the *Long* and *Short* conformations with the corresponding Boltzman weights. The PDF curves at temperatures 298(K), 500(K) and 800(K) were obtained by the convolution of PDFs from the MD simulations with the Gaussians with the correction widths from the *Long* conformations. It follows from the figure that the PDFs in the region of $r < 3$ (Å) only slightly change in the considered interval of temperatures. The inset that shows the region of $3 < r < 6.5$ (Å) on a bigger scale shows how the flexibility of the molecule develops as temperature increases.

The region $3 < r < 6.5$ (Å) is the most interesting if the large scale molecular motion is under consideration. In this region our correction is not very significant for a single molecule. However, in order to compare the results of calculations with

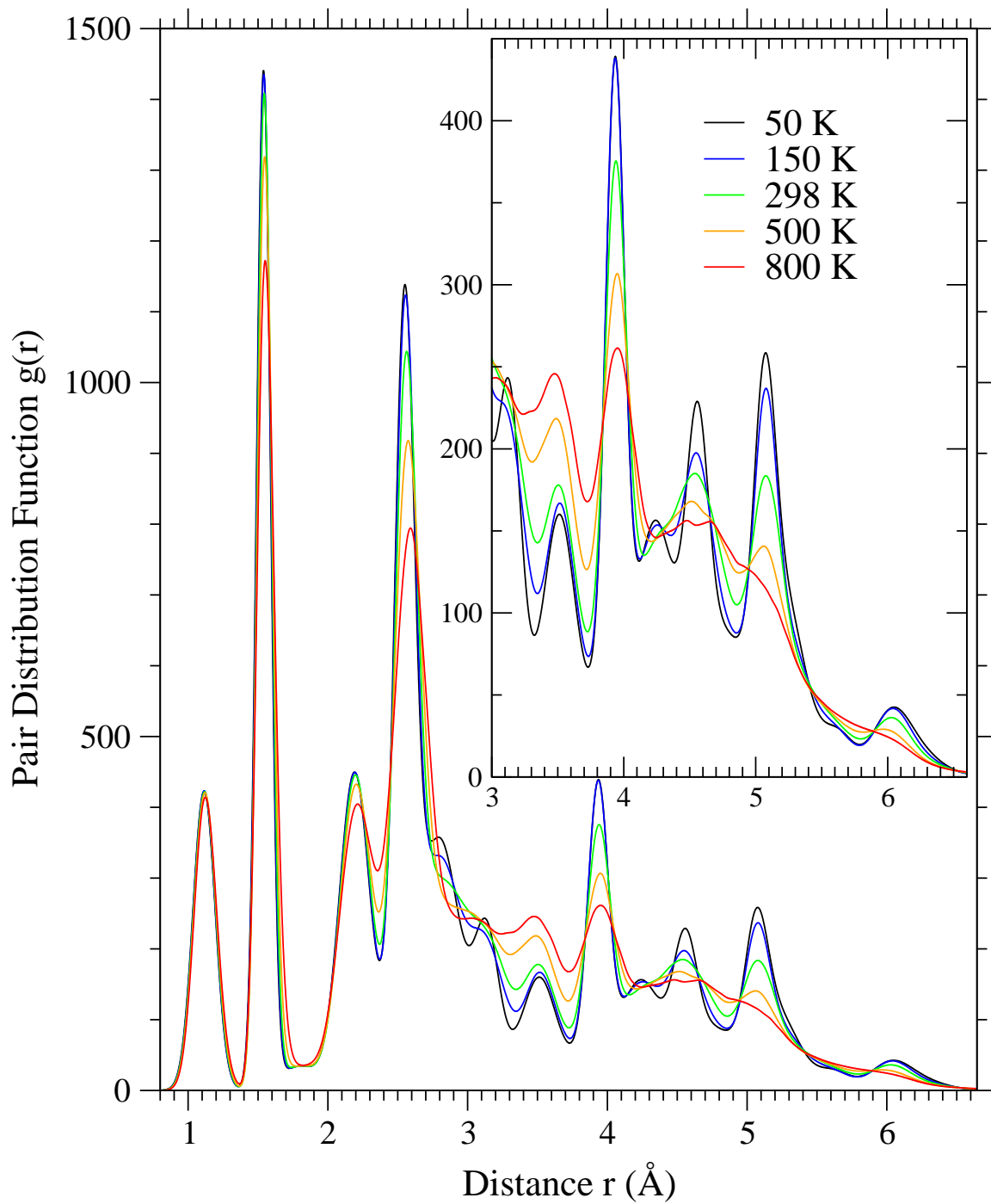


Figure 4.14: Corrected PDFs for the C_6H_{14} molecule at different temperatures. The inset shows the region between 3 \AA and 6.5 \AA on a bigger scale.

the experimental results, it is necessary to calculate the combined PDF from many different molecules. The PDF from the different molecules can overlap in the region $r < 3$ (Å). Thus, in order to extract accurate information about the mutual orientation of different molecules, (that in addition can put some constraints on a single molecular motion), it will be necessary to accurately calculate the PDF at small distances, i.e. in the region where our correction is significant.

4.6.3 Correction to the Heat Capacitance for C_6H_{14} molecule

Figure 4.15 shows the dependencies of the total energy (top panel) and the heat capacitance (bottom panel) of the C_6H_{14} molecule on temperature.

At low temperatures ($T < 150K$), the change between the *Long* and *Short* conformations does not occur. In the beginning of every simulation run the molecule was in one of the equilibrium conformations. Solid curves are for the molecule in the *Long* conformation, while dotted curves are for the molecule in the *Short* conformation. Solid and dotted curves are nearly identical.

The MD simulations were performed with the time step 1 femtosecond. The results of the MD simulations are shown in Fig. 4.15 as the orange curve on the top panel. The Tinker MD package provides the energies values averaged over 100 MD steps (0.1 picosecond). The total simulation time used to calculate the average energy values, was 1000 picoseconds. Thus, the average energy values were found by averaging over 10,000 different energy values, that are themselves are the average values over 100 MD steps. The MD simulations were performed at temperatures between 10 K and 1000 K with the temperature at different temperatures with the step in temperature 10 K .

To obtain the heat capacitance from MD simulations (the orange curve on the bottom panel), the derivatives of the energy curves (4.39) were calculated numerically with a temperature step 20 K. As follows from the figure, the precision with which heat

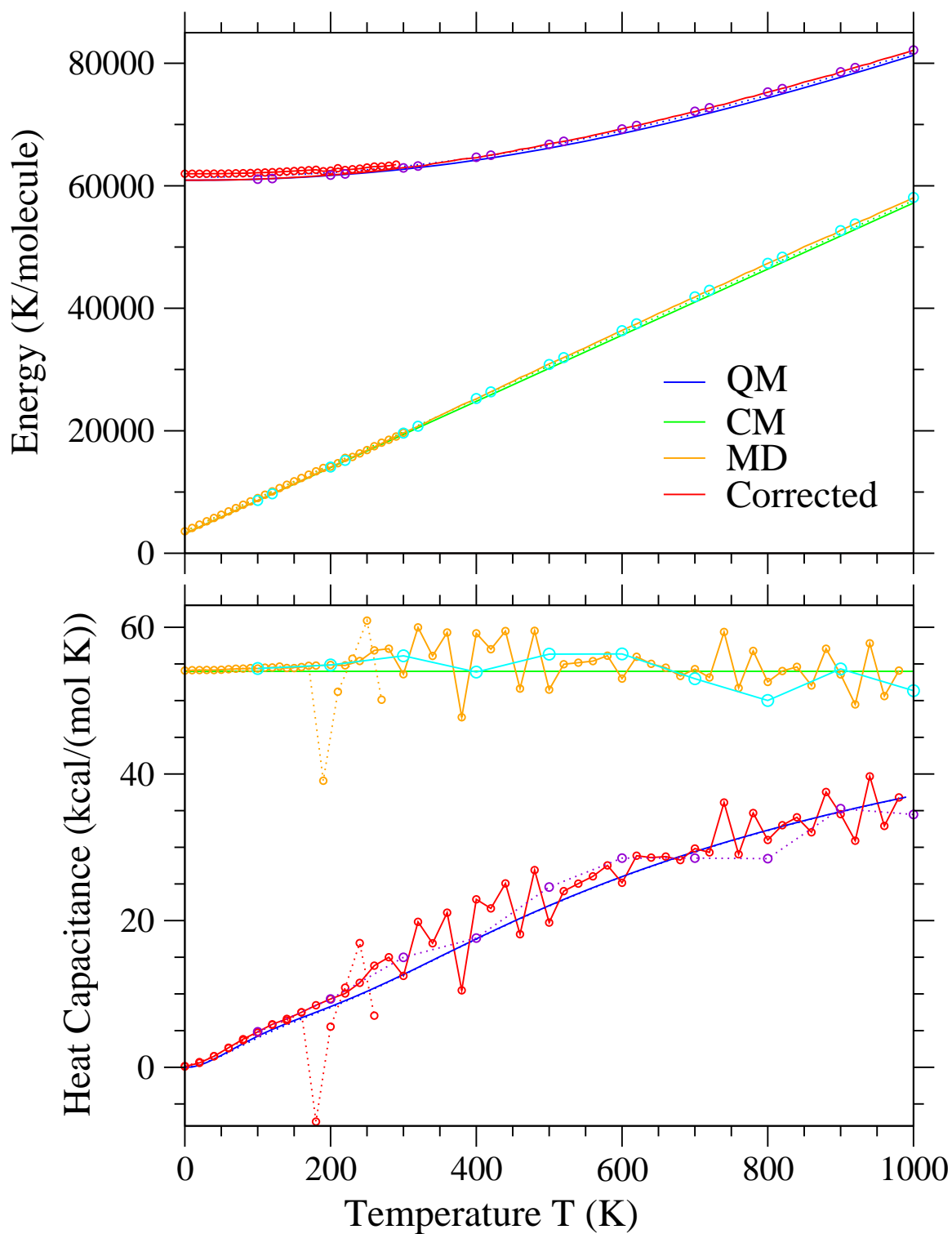


Figure 4.15: The dependencies of the vibrational energy and the vibrational heat capacitance on temperature for the C_6H_{14} molecule. Blue and green curves represent the QM and CM results for the harmonic approximation to the real potential. The orange curves and cyan dots represent the result of the MD simulations. The red curves show the corrected MD results. See more detailed description of the figure in the text.

capacitance is calculated significantly decreases when the molecule becomes flexible (i.e. when temperature is above 200 K).

In another approach the heat capacitance can be calculated from the energy fluctuations using the formula:

$$C = \frac{1}{T} \frac{(\langle E^2 \rangle - \langle E \rangle^2)}{k_b T}. \quad (4.65)$$

However, it cannot be applied directly to the results of the MD simulations that we have because the “TINKER” MD program produces as an output the energy values averaged over the 100 MD steps. Since at high temperatures the distribution of the energies for the C_6H_{14} molecule is clearly non-Gaussian, we can not easily correct the width of the distribution by multiplying it by some constant factor.

One way to overcome this difficulty (besides modifying the code of the program) is to run MD program for a very long time with a very small time step. In this case, averaging over 100 consecutive energy values should not have an effect.

It was verified that the time step 0.01 femtoseconds is sufficiently small for $T = 100K$. Additional simulations were made starting from the molecule in the *Long* conformation. The total simulation time was 3000 and 2000 picoseconds that was sufficient to obtain smooth energy distribution curves. The average energy values, obtained from these runs are shown as cyan circles in the top panel of Fig. 4.15.

The values of the heat capacitance, obtained from the fluctuation formula (4.65), turn out to be unreasonably small, approximately two orders of magnitude smaller than expected.

The values of the heat capacitance, obtained by differentiation (4.39) from these longer MD runs, are shown as cyan circles in the bottom panel. The corrected data for the energy and the heat capacitance are shown as violet dotted curves with circles in both panels.

The natural way to overcome the disagreement between the heat capacitances obtained by the differentiation (4.39) and from the fluctuation formula (4.65), would be to modify the code of the program in such a way that it would provide the energy values after every MD step. It would allow us, at least, to avoid ambiguities associated with the different tricks like multiplication by a constant factor or enormous decrease in the time step.

4.7 Conclusion

In this work in an attempt to develop an accurate technique for the calculation of PDF for flexible molecules we studied the role of quantum effects that are usually ignored in traditional Monte Carlo or Molecular Dynamics simulations. We found that it is very important to take into account the effect of zero-point motion, if an accurate PDF at small distances is desired. We developed a method that allows us to incorporate the effect of zero-point motion into the PDF, calculated classically from Monte Carlo or Molecular Dynamics molecular trajectories, and thus correct the classical PDF. We found that at large distances, especially when the molecule becomes flexible, its motion is almost classical.

In calculations of the total PDF for a conglomerate of molecules that are necessary to make the comparison with the experimental measurements, interactions between different molecules can be treated classically, since inter-molecular interactions are much weaker than intra-molecular interactions. Thus, the situation with inter-molecular interaction is analogous to the intra-molecular at large distances. Our correction is important if an accurate PDF in the whole range of distances is desired. It can help in reconstruction of the mutual orientations of different molecules, and thus to determine possible constrains that can be caused by the intermolecular interactions.

Appendix B

Cut-off for the Morse potential

In order to find σ_{MCM}^2 and $\langle U(T) \rangle$ for the Morse potential, it is necessary to perform integrations (4.14, 4.17, 4.38) with the Morse potential used as $U(x)$. For the Morse potential as $r \rightarrow \infty$ the value of potential goes to *const*, i.e. $\exp[-U(x)/(k_bT)]$ also goes to *const*. Thus the integrals under consideration diverge as $r \rightarrow \infty$. This divergence means that in infinite time, a particle would escape from the potential at any temperature. Due to this divergence it is unclear what should be the upper limit of the integration. However, if temperature is low enough, there is a range of upper cut-offs (sufficiently big, but not too big) that would lead to the same results with respect to $\sigma_{MCM}^2(T)$ and $\langle U_{MCM}(T) \rangle$.

Figure B.1 shows dependencies of $\sigma_{MCM}^2(T)$ and $\langle U_{MCM}(T) \rangle$ on temperature for different values of cut-off. Thus, we see that if $T \leq 10000$ K any reasonable value of cut-off leads to the basically the same results. Thus for the curves on the Fig.4.4, 4.5, 4.6 cut off 2.5 (Å) was used.

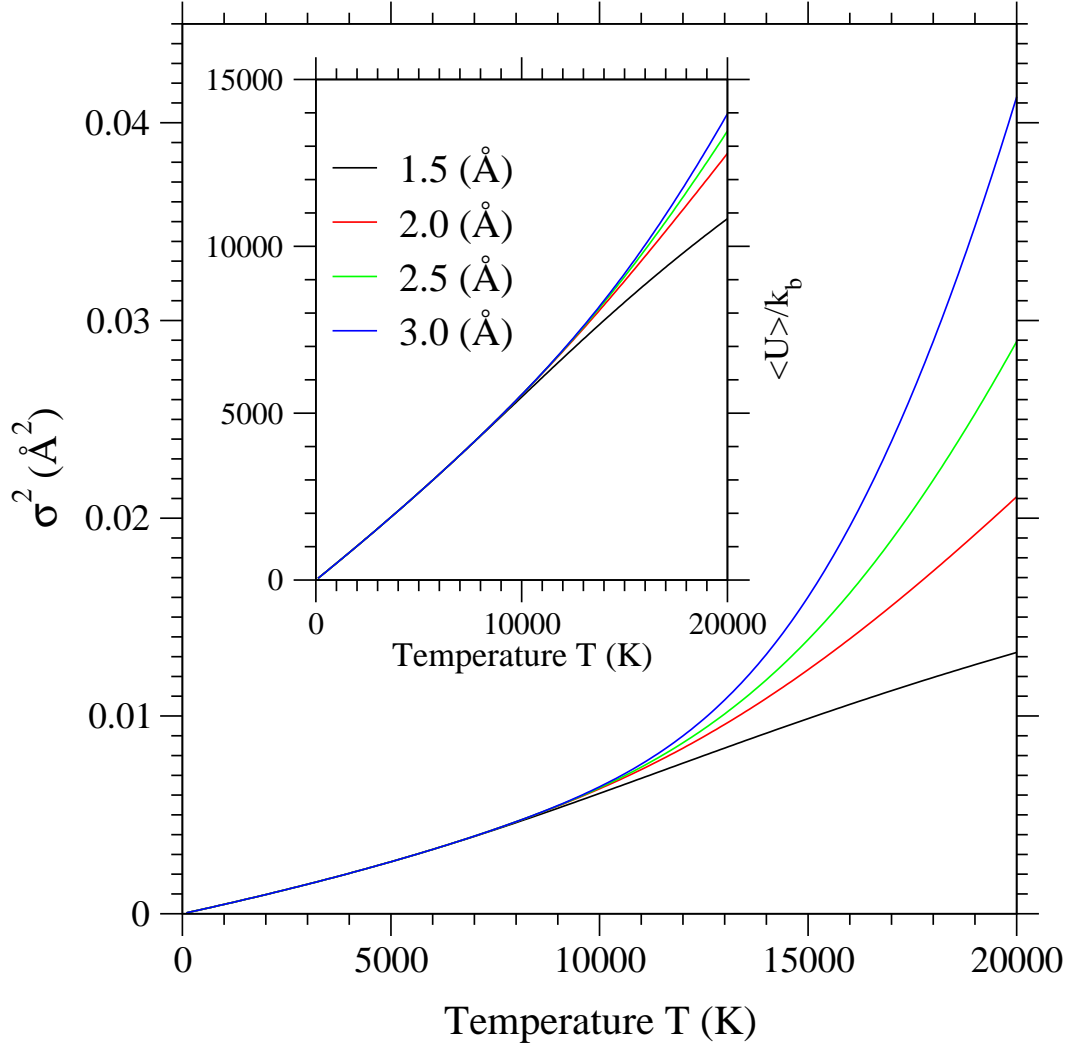


Figure B.1: Dependencies of $\sigma^2_{MCM}(T)$ on temperature (see Fig.4.4) for different values of the upper cut off in the integrals (4.14, 4.17). Thus, if $T \leq 10000$ (K) any cut-off in the interval (1.5:3.0) \text{\AA} would lead to basically the same result. The inset shows how $\langle U_{MCM}(T) \rangle$ (in temperature units) depends on temperature. Thus for the potential energy any upper cut off (see (4.38)) in the interval (1.5:3.0) \text{\AA} is also suitable.

Bibliography

- [1] Y. Xiao, M. F. Thorpe and J. B. Parkinson, *Phys. Rev. B* **59**, 277 (1999).
- [2] V.A. Levashov, M. F. Thorpe and B. W. Southern, *Phys. Rev. B* **67**, 224109 (2003).
- [3] H.F.W. Taylor, *Mineral. Mag.* **39**, 377 (1973).
- [4] D.L. Bish and G.W. Brindley, *Am. Miner.* **62**, 458 (1977).
- [5] G.W. Brindley and S. Kikkawa, *Am. Miner.* **64**, 836 (1979)
- [6] S.A. Solin, D.R. Hines, G.T. Seidler and M.M.J. Treacy, *J. Phys. Chem. Solids* **57**, 1043 (1996)
- [7] D.R. Hines, G.T. Seidler, M.M.J. Treacy and S.A. Solin, *Solid State Commun.* **101**, 835 (1997).
- [8] S.A. Solin, D.R. Hines, S.K. Yuk, T.J. Pinnavaia and M.F. Thorpe, *J. Non-Crystal. Solids* **182**, 212 (1995).
- [9] A. Audemer, A. Delahaye, R. Farhi, N. SacEpee and J.M. Tarascon, *J. Electrochem. Soc.* **144**, 2614 (1997).
- [10] S.U. Falk and A.J. Salkind, *Alkaline Storage Batteries*, Wiley, New York, 1969.
- [11] R. Barnard and C.F. Randell, *J. Appl. Electrochem.* **13**, 97 (1983).
- [12] A.D. Vidal and M. Figlarz, *J. Appl. Electrochem.* **17**, 589 (1987).
- [13] P. Elumalai, H.N. Vasan and N. Munichandraiah, *J. Power Sources* **93**, 201 (2001).
- [14] B. Liu, X.Y. Wang, H.T. Yuan, Y.S. Zhang, D.Y. Song and Z.X. Zhou, *J. Appl. Electrochem.* **29**, 855 (1999)
- [15] C. Faure, C. Delmas and P. Willmann, *J. Power Sources* **36**, 497 (1991).
- [16] G.A. Caravaggio, C. Detellier and Z. Wronski, *J. Mater. Chem.* **11**, 912 (2001).
- [17] F.Ducastelle, *Order and Phase Stability in Alloys*, Elsevier Science Publishers B.V. Amsterdam, The Netherlands, 1991.

- [18] A.J. Berlinsky, W.G. Unruh, W.R. McKinnon and R.R. Haering, *Solid. State. Commun.* **31**, 135 (1979).
- [19] W. Li, J.N. Reimers and J.R. Dahn, *Phys. Rev. B* **46**, 3236 (1992).
- [20] A.H. Thompson, *J. Electrochem. Soc.* **126**, 608 (1979).
- [21] M. Winter, J.O. Besenhard, M.E. Spahr and P. Novak, *Adv. Mater.* **10**, 725 (1998).
- [22] T. Zheng and J.R. Dahn, *Phys. Rev. B* **56**, 3800 (1997).
- [23] S.A. Safran and D.R. Hamann, *Phys. Rev. B* **22**, 606 (1980).
- [24] S.A. Safran and D.R. Hamann, *Phys. Rev. Lett.* **42**, 1410 (1979).
- [25] H.A. Kramers and G.H. Wannier, *Phys. Rev.* **60**, 252 (1941).
- [26] M. E. J. Newman and G.T. Barkema, *Monte Carlo Methods in Statistical Physics*, Oxford University Press Inc., New York, 1999.
- [27] A.C. Maggs and V. Rossetto, *Phys. Rev. Lett.* **88**, 196402 (2002).
- [28] E.P. Wigner, *Phys. Rev.* **46**, 1002 (1934).
- [29] G. Meissner, H. Namaizawa and M. Voss *Phys. Rev.* **13**, 4 (1976).
- [30] L. Bonsall and A.A. Maradudin, *Phys. Rev. B* **15**, 1959 (1977).
- [31] This exact result only agrees with the approximate expression in equation (11) of reference[1] in the limit $x \rightarrow 0$
- [32] F. Zernicke, J.A. Prins *Zeit Physik.* **41**, 184- (1927).
- [33] P.J.W. Debye, H. Menke *Physical. Zeit.* **31**, 797 (1930).
- [34] B.E. Warren *X-ray diffraction* (Addison-Wesley Publishing Company).
- [35] J.S. Chung, M.F. Thorpe Local atomic structure of semiconductor alloys using pair distribution function *Phys. Rev. B* **59**, 1545-1553 (1997).
- [36] M.F. Thorpe, J.S.Chung, J.S.L. Billinge and F. Mohiuddin-Jacobs *Advances in Pair Distribution Profile Fitting in Alloys in Local Structure from Diffraction*, 157-174, Ed. By S.J.L. Billinge and M.F. Thorpe (Plenum Press, New York, 1998)
- [37] M.F. Thorpe, V.A. Levashov, M. Lei and S.J.L. Billinge *Notes on the analysis of data for pair distribution functions*, 105-128, Ed. By S.J.L. Billinge and M.F. Thorpe (Kluwer Academic/Plenum Publishers, New York, 2002)
- [38] D.A. Dimitrov, H. Rder and A.R. Bishop *Phys. Rev. B* **64**, 14303 (2001)

- [39] B.H. Toby and T. Egami *Acta Cryst.* **48**, 336 (1992)
- [40] For a summary on Lattice Point Theory, see <http://mathworld.wolfram.com/PointLattice.html>
- [41] E. Krätzel *Lattice Points*, Kluwer Academic Publishers (1988)
- [42] P. Erdős, P.M. Gruber, and J. Hammer *Lattice Points*, Longman Scientific and Technical with John Wiley and Sons, Inc., New York (1989)
- [43] C.F. Gauss *De nexu inter multitudinem classium, in quas formae binariae secundi gradus distribuuntur, earumque determinantem.* *Werke*, vol.2, pp.269-291 (277)
- [44] For a summary of what is known about the Gauss Circle Problem, see <http://mathworld.wolfram.com/GaussCircleProblem.html>
- [45] L.D. Landau, E.M. Lifshitz *Statistical Physics P1* (1999)
- [46] S. Torquato, T.M. Truskett and P.G. Debenedetti *Is Random Close Packing of Spheres Well Defined?* *Phys. Rev. Lett.*, **84**, 2064 (2000)
- [47] W.M. Visscher and M. Bolsterli *Nature (London)* **239**, 504 (1972) See also remarks published in *Nature (London)* **239**, 488 (1972)
- [48] J. Tobochnik and P.M. Chapin *J. Chem. Phys.* **88**, 5824 (1988).
- [49] F. Wooten, K. Winer, D. Weaire *Phys. Rev. Lett.* **54**, 1392 (1985).
- [50] H. He Ph.D. thesis, Michigan State University (1985).
- [51] G.T. Barkema and N. Mousseau *High-quality continuous random networks.* *Phys. Rev. B* **62**, 4985-4990 (2000).
- [52] R.L.C. Vink, G.T. Barkema, M.A. Stijnman and R.H. Bisseling *Towards device-size computer models of amorphous silicon.* *Phys. Rev. B* **64**, 245214 (2001).
- [53] M.N. Huxley *Exponential Sums and Lattice Points.* *Proc.London Math. Soc.* **60**, 471-502, 1990
- [54] G. H. Hardy *Quart. J. Math.* **46**, 283, 1915
- [55] E. Landau *Über die Gitterpunkte in einem Kreise.* (Zweite Mitteilung.) *Nachrichten der K. Gesellschaft der Wissenschaften zu Göttingen. Mathematisch-physikalische Klasse.* 161-171 (1915).
- [56] P.M. Bleher *Duke Mathematical Journal* **67**, No.3 p.461
- [57] P.M. Bleher, F.J. Dyson and J.L. Lebowitz *Non-Gaussian energy level statistics for some integrable systems* *Phys. Rev. Lett.* **71**, No.19 p.3047-3050 (1993)
- [58] B.E. Warren *X-ray diffraction* (Addison-Wesley Publishing Company).

- [59] J.S. Chung, M.F. Thorpe Local atomic structure of semiconductor alloys using pair distribution function Phys. Rev. B **59**, 1545-1553 (1997).
- [60] R. Car and M. Parinello Unified Approach for Molecular Dynamics and Density-Functional Theory, Phys. Rev. Lett. **55**, p.2471-2474 (1985)
- [61] M. J. Frisch, G. W. Trucks, H. B. Schlegel, G. E. Scuseria, M. A. Robb, J. R. Cheeseman, V. G. Zakrzewski, J. A. Montgomery, Jr., R. E. Stratmann, J. C. Burant, S. Dapprich, J. M. Millam, A. D. Daniels, K. N. Kudin, M. C. Strain, O. Farkas, J. Tomasi, V. Barone, M. Cossi, R. Cammi, B. Mennucci, C. Pomelli, C. Adamo, S. Clifford, J. Ochterski, G. A. Petersson, P. Y. Ayala, Q. Cui, K. Morokuma, P. Salvador, J. J. Dannenberg, D. K. Malick, A. D. Rabuck, K. Raghavachari, J. B. Foresman, J. Cioslowski, J. V. Ortiz, A. G. Baboul, B. B. Stefanov, G. Liu, A. Liashenko, P. Piskorz, I. Komaromi, R. Gomperts, R. L. Martin, D. J. Fox, T. Keith, M. A. Al-Laham, C. Y. Peng, A. Nanayakkara, M. Challacombe, P. M. W. Gill, B. Johnson, W. Chen, M. W. Wong, J. L. Andres, C. Gonzalez, M. Head-Gordon, E. S. Replogle, and J. A. Pople, Gaussian, Inc., Pittsburgh PA, 2001.
- [62] M.J.S. Dewar, E.G. Ziegler and E.F. Healy Gaussian 98, Revision A.11.1, J. Amer. Chem. Soc. **107**, 3902 (1985)
- [63] L.D.Landau and E.M. Lifshits Quantum Mechanics: Non-Relativistic Theory, Volume 3, Butterworth-Heinemann; 3rd edition (February 1997)
- [64] L.D.Landau and E.M. Lifshits Statistical Physics, Volume 5, Butterworth-Heinemann; 3rd edition, Part 1 (February 1999)
- [65] P.M. Morse Phys. Rev. **34** 57-64 (1929)
- [66] N. L. Allinger, Y. H. Yuh and J.-H. Lii, "Molecular Mechanics. The MM3 Force Field for Hydrocarbons. 1", J. Am. Chem. Soc., **111**, 8551-8566 (1989)
- [67] J.-H. Lii and N. L. Allinger, "Molecular Mechanics. The MM3 Force Field for Hydrocarbons. 2. Vibrational Frequencies and Thermodynamics", J. Am. Chem. Soc., **111**, 8566-8575 (1989)
- [68] J.-H. Lii and N. L. Allinger, "Molecular Mechanics. The MM3 Force Field for Hydrocarbons. 3. The van der Waals' Potentials and Crystal Data for Aliphatic and Aromatic Hydrocarbons", J. Am. Chem. Soc., **111**, 8576-8582 (1989)
- [69] N. L. Allinger, H. J. Geise, W. Pyckhout, L. A. Paquette and J. C. Gallucci, "Structures of Norbornane and Dodecahedrane by Molecular Mechanics Calculations (MM3), X-ray Crystallography, and Electron Diffraction", J. Am. Chem. Soc., **111**, 1106-1114 (1989) [torsion-stretch]
- [70] N. L. Allinger, F. Li and L. Yan, "Molecular Mechanics. The MM3 Force Field for Alkenes", J. Comput. Chem., **11**, 848-867 (1990)

- [71] N. L. Allinger, F. Li, L. Yan and J. C. Tai, "Molecular Mechanics (MM3) Calculations on Conjugated Hydrocarbons", *J. Comput. Chem.*, **11**, 868-895 (1990)
- [72] J.-H. Lii and N. L. Allinger, "Directional Hydrogen Bonding in the MM3 Force Field. I", *J. Phys. Org. Chem.*, **7**, 591-609 (1994)
- [73] J.-H. Lii and N. L. Allinger, "Directional Hydrogen Bonding in the MM3 Force Field. II", *J. Comput. Chem.*, **19**, 1001-1016 (1998)
- [74] See the Internet web-site of the "TINKER" program:
<http://dasher.wustl.edu/tinker/>
- [75] P. Ren and J. W. Ponder, *J. Phys. Chem. B*, **107**, 5933-5947 (2003)
- [76] R. V. Pappu, R. K. Hart and J. W. Ponder, *J. Phys. Chem. B*, **102**, 9725-9742 (1998)
- [77] M. E. Hodsdon, J. W. Ponder and D. P. Cistola, *J. Mol. Biol.*, **264**, 585-602 (1996)
- [78] M. J. Dudek and J. W. Ponder, *J. Comput. Chem.*, **16**, 791-816 (1995)
- [79] C. E. Kundrot, J. W. Ponder and F. M. Richards, *J. Comput. Chem.*, **12**, 402-409 (1991)
- [80] J. W. Ponder and F. M. Richards, *J. Comput. Chem.*, **8**, 1016-1024 (1987)